Dr. Steffen M. Diebold

Physiological Parameters Relevant to Dissolution Testing

Hydrodynamic Considerations

(revised and supplemented version)

Content Outline

I Hydrodynamics and dissolution

1 Dissolution

Why is hydrodynamics relevant to dissolution testing?

Release-related bioavailability problems have been encountered in the pharmaceutical development of formulations for a number of quite different chemical entities, including ciclosporin, digoxin, griseofulvin and itraconazole, to name but a few. A thorough knowledge of hydrodynamics is useful in the course of the dissolution method development, in the course of formulation development as well as for the pharmaceutical industry's quality needs, e.g. the batch to batch control. Occasionally, quality control specifications are not met due to "minor" variations involving hydrodynamics such as the use of different volumes, modified stirring devices or sampling procedures. The development of the drug formulation is facilitated by the choice of an appropriate dissolution apparatus based on insight into its specific hydrodynamic performance. Using the right test might make it easier, for instance, to isolate the impact of different excipients and process parameters on the drug release in an early stage of pharmaceutical formulation development. Furthermore, a sound knowledge of *in vivo* hydrodynamics may help to better understand and possibly to improve forecasting of *in vivo* dissolution and absorption of BCS II compounds. Although gastrointestinal fluids are well characterized and biorelevant dissolution media (e.g. FaSSIF and FeSSIF) have been developed to simulate various states in the GI tract, knowledge of hydrodynamics appears to be relatively scant both *in vitro* and *in vivo*. The chapter gives a brief introduction into basic hydrodynamics relevant to *in vitro* dissolution testing including the convective diffusion theory. This section is followed by hydrodynamic considerations of *in vitro* dissolution testing and hydrodynamic problems inherent to *in vivo* bioavailability of solid oral dosage forms.

The dissolution process

Dissolution can be described as a mass transfer process. Although mass transfer processes commonly are under the combined influence of both the thermodynamics and the hydrodynamics, usually one of these prevails in terms of the overall dissolution process [1-3]. Hydrodynamics is predominant for the overall dissolution rate if the mass transfer process is *mainly* controlled by convection and/or diffusion, as is usually the case for poorly soluble

substances. This is of great practical relevance for pharmaceutical development since new drug compounds often exhibit poor solubility in aqueous media.

The dissolution rate

The dissolution rate (dC/dt) of a pure drug compound is represented by an equation based on the work of Noyes, Whitney, Nernst and Brunner [4-6], which is in turn based on earlier observations made by Schükarew in 1891 [7]:

$$\frac{dC}{dt} = \frac{A \cdot D}{\delta_{HL} \cdot V} \cdot (Cs - Ct)$$

The proportionality constant k

$$k = \frac{A \cdot D}{\delta_{HL} \cdot V}$$

is addressed as the "apparent dissolution rate constant". Cs represents the saturation solubility, Ct describes the bulk concentration of the dissolved drug at time (t), D characterizes the effective diffusion coefficient of the drug molecule, A stands for the surface area available for dissolution and V represents the media volume employed in the test. According to the equations of Noyes, Whitney, Nernst and Brunner the dissolution rate depends on a small fluid "layer", called the "hydrodynamic boundary layer" (δ_{HL}), adhering closely to the surface of a solid particle that is to be dissolved (solvendum, solute). As can be seen from the combined equation an inverse proportionality exists between the dissolution rate and the hydrodynamic boundary layer. If the latter is reduced, the dissolution rate increases.

2 Hydrodynamic basics relevant to dissolution

Laminar and turbulent flow

Laminar flow is characterized by layers ("*lamellae*") of liquid moving at the same speed and in the same direction. Little or no exchange of fluid mass and fluid particles occurs across these fluid layers. The closer the layers are to a given surface, the slower they move. In an

ideal fluid, the flow follows a curved surface smoothly, with the layers central in the flow moving fastest and those at the sides slowest. In turbulent flow, by contrast, the streamlines or flow patterns are disorganized and there is an exchange of fluid between these areas. Momentum is also exchanged such that slow moving fluid particles speed up and fast moving fluid particles give up their momentum to the slower moving particles and slow down themselves. All, or nearly all, fluid flow displays some degree of turbulence. If the fluid velocity exceeds a crucial number, flow becomes turbulent rather than laminar since the frictional force can no longer compensate for other forces acting on the fluid particles. This event depends on the fluid viscosity, the fluid velocity and the geometry of the hydrodynamic system and is described by the Reynolds number.

Fig. 1

Reynolds number

The dimensionless Reynolds number (Re) is used to characterize the laminar-turbulent transition and is commonly described as the ratio of momentum forces to viscous forces in a moving fluid. It can be written in the form:

$$\mathrm{Re} = \frac{\rho \cdot U_A \cdot L}{\eta} = \frac{U_A \cdot L}{\nu}$$

where (ν) represents the kinematic viscosity of the liquid (ρ and η are the density and the dynamic viscosity, respectively). U_A describes the flow rate and L represents a characteristic distance or length of the hydrodynamic system, for example the diameter of a tube or pipe. Laminar flow patterns turn into turbulent flow if the Reynolds number of a particular hydrodynamic system exceeds a *critical* Reynolds number (Re_{crit}).

Particle-liquid Reynolds numbers

With respect to the hydrodynamics of particles in a stirred dissolution medium, the Reynolds numbers determined for the bulk flow have to be distinguished from the Reynolds numbers characterizing the particle-liquid system. The latter hydrodynamic sub-system consists of the dissolving particles and the surrounding fluid close to their surfaces. Thus, it is the relative velocity of the solid particle surface to the bulk flow (the “slip velocity”) that counts.

However, it is permissible to approximate the slip velocity to U_A, provided that the drug particles are suspended in the moving fluid and the density difference between particle and dissolution medium is at least ~0.3 g/cm^3 [8]. In this case, L represents a characteristic length on the (average) particle surface and may arbitrarily be identified with the particle diameter. With respect to particle-liquid systems, the laminar-turbulent transition at the particle surface is decisive. Laminar flow turns into turbulent if the critical Reynolds number Re_{crit} for the flow *close to the particle surface* is exceeded. Thus, Re_{crit} (particle) is not necessarily identical with the Reynolds number of the bulk flow - although the latter may sometimes serve as an sufficient approximation [9, 10].

„Eddies“, dissipation and energy cascade

„Eddies“ are turbulent instabilities within a flow region. These vortices might already be present in a turbulent stream or can be generated downstream by an object presenting an obstacle to the flow. The latter turbulence is known as “Karman vortex streets”. Eddies can contribute a considerable increase of mass transfer in the dissolution process under turbulent conditions and may occur in the GI tract as a result of short bursts of intense propagated motor activity and flow “gushes”.

Fig. 2

The mean velocity of eddies changes at a definitive distance called the „scale of motion“ (SOM) [11]. The bigger these eddies are, the longer is the scale of motion ([9], § 4). Apart from „large scale eddies“ a number of „small scale eddies“ exist in turbulent flow. Under turbulent conditions eddies transport the majority of the kinetic energy. Energy fed into the turbulence goes primarily into the larger eddies. From these, smaller eddies are generated, and then stil1 smal1er ones. The process continues until the length scale is small enough for viscous action to be important and dissipation to occur. This sequence is cal1ed the energy cascade. At high Reynolds numbers the cascade is long; i.e. there is a large difference in the eddy sizes at its ends. There is then little direct interaction between the large eddies governing the energy transfer and the small, dissipating eddies. In such cases the dissipation is determined by the rate of supply of energy to the cascade by the large eddies and is independent of the dynamics of the small eddies in which the dissipation actually occurs. The rate of dissipation is independent of the magnitude of the viscosity. An increase in the

Reynolds number to a still higher value extends the cascade only at the small eddy end. Still, smaller eddies must be generated before dissipation can occur.

Energy input (ε)

For closed dissolution systems it can be hypothesized that the hydrodynamics depends on the input of energy in a general way. The energy input may be characterized by the power input per unit mass of fluid or the „turbulent energy dissipation rate per unit mass of fluid“ (ε). Considering various *paddle* apparatus, the power input per unit mass of fluid can be calculated according to Plummer ([12], App. B, nomenclature adapted).

$$\varepsilon = \frac{p \cdot I^5 \cdot \omega^3}{V}$$

where ε has the dimension (length^2/time^3). ω stands for the rotations per minute, I is the mean diameter of the paddle or impeller, p is a model constant depending of the hydrodynamic flow pattern (laminar or turbulent) and V is the fluid volume. As expected, ε is influenced mainly by the diameter of the impeller and the rotation rate. Based on this equation, the power input per unit mass of fluid for the compendial paddle apparatus has been calculated ([10], chapter 5.6.2). The fluid mass specific energy input rises exponentially with paddle speed. The exponential form of the observed relationship suggests that there is a transition from laminar (p=0.5) to turbulent flow (p=1.0) within the system, and indicates that the energy input to the media and flow pattern in the vessels are related.

Fig. 3

The power input per unit mass of fluid is greater for a dissolution volume of 500 ml than for 900 ml, at a given stirring rate. Remarkably, ε calculated for laminar conditions (p=0.5) employing 500 ml of dissolution medium (not plotted) results in approximately the same hydrodynamic effectiveness as when turbulent conditions are assumed (p=1.0) for a dissolution volume of 900 ml [10]. This implies more effective hydrodynamics for the lower volume. Thus, it *cannot* be assumed that there are no hydrodynamic implications when volumes used for a specific dissolution tests method are changed, rather, that the change would require meticulous validation!

3 Hydrodynamic boundary layer concept

Concept and structure of the boundary layer

A boundary layer in fluid mechanics is defined as the layer of fluid in the immediate vicinity of a limiting surface where the layer and its breadth are affected by the viscosity of the fluid. The concept of the hydrodynamic boundary layer goes back to the work of the German physicist and mathematician Ludwig Prandtl (1875-1953) and was first presented at Göttingen and Heidelberg in 1904. According to the Prandtl concept, at high Reynolds numbers the flow close to the surface of a body can be separated in two main regions. Within the bulk flow region viscosity is negligible ("frictionless flow") whereas near to the surface a small region exists that is called the hydrodynamic boundary layer. In this region, adherence of the molecules of the liquid to the surface of the solid body slows them down. The hydrodynamic boundary layer is dominated by pronounced velocity gradients within the fluid that are continuous, and does not, as is sometimes purported, consist of a stagnant layer. According to Newton's law of friction, pronounced velocity gradients lead to high friction forces near the surface of a solid particle. The hydrodynamic boundary layer grows further downstream of the surface since more and more fluid molecules are slowed down.

Fig. 4

In terms of hydrodynamics the boundary layer *thickness* is measured from the solid surface (in the perpendicular direction from a particle's surface, for instance) to an arbitrarily chosen point, e.g., where the velocity is 90 to 99 percent of the stream velocity or the bulk flow (δ_{90} or δ_{99}, respectively). Thus, the breadth of the boundary layer depends *ad definitionem* on the selection of the reference point and includes the laminar boundary layer as well as possibly a portion of a turbulent boundary layer.

Laminar and turbulent boundary layer

Apart from the nature of the bulk flow, the hydrodynamic scenario close to the surfaces of drug particles have to be considered. The nature of the hydrodynamic boundary layer generated at the particle's surface may be laminar or turbulent regardless of the bulk flow characteristics. The turbulent boundary layer is considered to be thicker than the laminar

layer. Nevertheless, mass transfer rates are usually increased with turbulence due to the presence of the “viscous turbulent sub-layer”. This is the part of the (total) turbulent boundary layer that constitutes the main resistance to the overall mass transfer in the case of turbulence. The development of a viscous turbulent sub-layer reduces the overall resistance to mass transfer since this viscous sub-layer is much narrower than the (total) laminar boundary layer. Thus, mass transfer from turbulent boundary layers is greater than would be calculated according to the total boundary layer thickness.

Boundary layer separation

Both laminar and turbulent boundary layers can separate. Laminar layers usually require only a relatively short region of adverse pressure gradient to produce separation whereas turbulent layers separate less readily. A few examples of turbulent boundary layer separation include golf ball design to stabilize the trajectory, airfoil design to reduce the aerodynamic resistance and, in nature, in sharkskin to improve the shark’s ability to glide. The overall flow pattern, when separation occurs, depends greatly on the particular flow. The flow upstream of the separation point is fed by recirculation of some of the separating fluid. Sometimes the effect is quite localized but more often it is not. The consequent post-separation pattern is affected by the fact that the separated flow becomes turbulent and so there is a highly fluctuating recirculation motion over the whole surface of the body. With respect to the dissolution of drug particles from oral solid formulations, recirculation flow is expected to increase mass transfer and can take place even at low Reynolds numbers of Re~10 [13].

Fig. 5

As mentioned, a laminar boundary layer separates a greater distance from the surface of a curved body than a turbulent one. The laminar boundary layer in the upper photo is shown separating from the crest of the convex surface, while the turbulent boundary layer in the second photo remains attached longer, with the point of separation occurring further downstream. Turbulent layer separation occurs when the Reynolds stresses are much larger than the viscous stresses.

Prerequisites of the hydrodynamic boundary layer concept

Originally, the concept of the Prandtl boundary layer was developed for *hydraulic „even“* bodies. It is assumed that any characteristic length L on the particle surface is much greater than the thickness (δ_{HL}) of the boundary layer itself ($L >> \delta_{HL}$). Provided this assumption is fulfilled, the concept can be adapted to curved bodies and spheres, including “real” drug particles. Furthermore, the classical (“macroscopic”) concept of the hydrodynamic boundary layer is valid solely for high Reynolds numbers of $Re>10^4$ [14, 15]. This constraint was overcome for the “microscopic” hydrodynamics of dissolving particles by the „convective diffusion theory“ [9].

4 The „convective diffusion theory“

The „convective diffusion theory“ was developed by V. G. Levich to solve specific problems in electrochemistry encountered with the rotating disc electrode. Later, he applied the classical concept of the boundary layer to a variety of practical tasks and challenges like particle-liquid hydrodynamics and liquid-gas interfacial problems. The conceptual transfer of the hydrodynamic boundary layer is applicable to the hydrodynamics of dissolving particles if the Peclet number (Pe) is greater than unity (Pe>1) [9]. The dimensionless Peclet number (Pe) describes the relationship between convection and diffusion driven mass transfer.

$$Pe = \frac{U_A \cdot L}{D}$$

D represents the diffusion coefficient. For example, low Peclet numbers indicate that convection contributes less to the total mass transfer and the latter is mainly driven by diffusion. In contrast, at high Peclet numbers mass transfer is dominated by convection. The quotient of Peclet- and Reynolds number (Re) is called the „Prandtl number” (Pr), or, if we are talking about diffusion processes, the “Schmidt number” (Sc):

$$Pr = \frac{Pe}{Re} = \frac{\nu}{D} = Sc$$

The Schmidt number is the ratio of kinematic viscosity to molecular diffusivity. Considering liquids in general and dissolution media in particular the values for the kinematic viscosity

usually exceed those for diffusion coefficients by a factor of 10^3 to 10^4. Thus, Prandtl or Schmidt numbers of about 10^3 are usually obtained. Subsequently, and in contrast to the classical concept of the boundary layer, Re numbers in the magnitude of about Re>=0.01 are sufficient to generate Peclet numbers greater than 1 and to justify the hydrodynamic boundary layer concept for particle-liquid dissolution systems (Re*Pr=Pe). It can be shown that ([9], term 10.15, nomenclature adapted):

$$\delta \approx D^{\frac{1}{3}} \cdot \nu^{\frac{1}{6}} \cdot \sqrt{\frac{L}{U_A}}$$

Note that the hydrodynamic boundary layer depends on the diffusion coefficient. Introducing the proportionality constant $K_e°$ results in an equation valid for any desired hydrodynamic system based on relative fluid motion as proposed by [10].

$$\delta_{HL} = K_e° \cdot D^{\frac{1}{3}} \cdot \nu^{\frac{1}{6}} \cdot \sqrt{\frac{L}{U_A}}$$

$K_e°$ consists of a combination of Prandtl's original proportionality constant used for the hydrodynamic boundary layer at a semi-infinitive plate, (K_e), and a constant (K°), characterizing a particular hydrodynamic system that is under consideration. The latter constant has to be determined experimentally.

$$K_e° = K_e \cdot K°$$

Among other factors, K° is influenced by the particle geometry and the surface morphology (roughness, edges, corners and defects). For instance, K° would equal 1 in the case of a smooth semi-infinite plate and in this case $K_e°$ is identical to K_e. Considering the „rotating disc system" in particular, Levich found K° to be 0.5. Given that a semi-infinite plate dissolves in a liquid stream and K_e equals 5.2 (which represents Prandtl`s proportionality constant in the case of a semi-infinite plate, thus $K_e°$=2.6) we arrive at the following term for the thickness of Levich's *effective* hydrodynamic boundary layer [10]:

$$\delta_{HL} = 2.6 \cdot D^{\frac{1}{3}} \cdot \nu^{\frac{1}{6}} \cdot \sqrt{\frac{L}{U_A}}$$

5 The combination model

A reciprocal proportionality exists between the square root of the characteristic flow rate U_A, and the thickness of the effective hydrodynamic boundary layer, δ_{HL}. Moreover, δ_{HL} depends on the diffusion coefficient D, on the characteristic length, L and on the kinematic viscosity ν of the fluid. Based on Levich's convective diffusion theory the "combination model" ("Kombinations-Modell") was derived to describe the dissolution of particles and solid formulations exposed to agitated systems [10, chapter 5.2]. In contrast to the rotating disc method, the combination model is intended to serve as an approximation describing the dissolution in hydrodynamic systems where the solid solvendum is not necessarily fixed but is likely to move within the dissolution medium. Introducing the term

$$\delta_{HL} = 2.6 \cdot D^{\frac{1}{3}} \cdot \nu^{\frac{1}{6}} \cdot \sqrt{\frac{L}{U_A}}$$

into the well known equation adapted from Noyes, Whitney, Nernst and Brunner (NWNB)

$$\frac{dC}{dt} = \frac{A \cdot D}{\delta_{HL} \cdot V} \cdot (Cs - Ct)$$

and employing the proportionality constant k as the apparent dissolution rate constant:

$$k = \frac{A \cdot D}{\delta_{HL} \cdot V}$$

results in the combination model according to Diebold [10].

$$\frac{dC}{dt} = 0.385 \cdot D^{\frac{2}{3}} \cdot \nu^{-\frac{1}{6}} \cdot \left(\frac{L}{U_A}\right)^{-\frac{1}{2}} \cdot \frac{A}{V} \cdot (Cs - Ct)$$

where Cs represents the saturation solubility of the drug, Ct describes the concentration of the dissolved drug in the bulk at time t, D stands for the effective diffusion coefficient of the dissolved compound, A represents the total surface area accessible for dissolution of the drug particles and V is the volume of the dissolution medium employed in the test. Note that the apparent dissolution rate constant k is now a function of the flow rate that a particle surface "sees" (slip velocity) and also a function of L, the characteristic length on the particle surface: k (U_A; L). The proportionality constant k can be determined by appropriately performed dissolution experiments or calculated using the following equation:

$$\ln(Cs - C_0) - \ln(Cs - Ct) = k \cdot t$$

where Co is the initial concentration of the drug at t equals zero. Since δ_{HL} is related to k as demonstrated above, the combination model permits calculation of an overall average hydrodynamic boundary layer δ_{HL} for a given particle size fraction. Thus, the proposed relationship provides a tool for *a priori* prediction of the average hydrodynamic boundary layer of non-micronized drugs and hence to roughly forecast (!) dissolution rate *in vitro* under well defined circumstances e.g. for the paddle apparatus ([10], chapter 5.5, pp. 61-62, chapters 12.3.8 and 13.4.10).

6 Further factors affecting the hydrodynamic boundary layer

Apart from the flow rate, of course, properties of the dissolution medium as well as the drug compound influence the effective hydrodynamic boundary layer and hence the intrinsic dissolution rate.

Saturation solubility (C_s)

Although the saturation solubility (C_s) influences the *apparent* dissolution rate constant it is an *intrinsic* property of a drug compound and can in so far affect the hydrodynamic boundary layer indirectly. High aqueous solubility, for example, leads to concentration-driven convection at the surface of the drug particles. Thus, forced and natural convection are mixed together and it is challenging to separate/forecast their hydrodynamic effects on dissolution rate. *In vivo* dissolution, however, offers additional problems to the control of hydrodynamics. The saturation solubility (Cs) of a drug in intestinal chyme may vary greatly

within the course of dissolution *in vivo* as has been demonstrated previously [10]. The *in vivo* solubility of felodipine in jejunal chyme (37°C), for example, was determined to be about 10 µg/ml on average (median), but varied greatly with time at mid-jejunum, ranging from 1 µg/ml to 25 µg/ml or even from 1 µg/ml to 273 µg/ml, depending on the conditions of administration [10]. Solubility variations within the course of an *in vivo* dissolution experiment may in such cases override hydrodynamic effects. Thus, the observed time dependency of intestinal drug solubility should be taken into account by dissolution models, which otherwise may describe dissolution rates *in vitro* well but fail to do so *in vivo*.

Diffusion coefficient (D)

The diffusion coefficient is linked to the intrinsic dissolution rate constant (k_i) as expressed by the term:

$$k_i = \frac{D}{\delta_{HL}}$$

Thus, the thickness of the effective hydrodynamic boundary layer δ_{HL} obviously depends on the diffusion coefficient. The diffusion coefficient D further correlates to the diameter of the particle or molecule as demonstrated by the relation of Stokes and Einstein:

$$D = \frac{\kappa_B \cdot T}{3 \cdot d \cdot \eta \cdot \pi}$$

where T is the temperature in (K) and κ_B represents the Boltzmann-Constant ($1.381*10^{-23}$ J/K). The term reveals that the diffusion coefficient D itself is dependent on the dynamic viscosity (η). In the gastrointestinal tract diffusion coefficients of drugs may be reduced due to alterations in the fluid viscosity. Larhed et al. reported that diffusion coefficients for testosterone were reduced by 58 % in porcine intestinal mucus [16]. It has also been observed in dissolution experiments that the reduction of diffusion coefficients can counteract effects of increased drug solubility due to mixed micellar solubilisation [17].

Kinematic viscosity (ν)

The viscosity of upper gastrointestinal fluids can be increased by food intake. The extent of this effect will depend on the food components and the composition and volume of co-administered fluids. Aqueous soluble fibres such as pectin, guar and some hemicelluloses are able to increase the viscosity of aqueous solutions. Increasing the kinematic viscosity of the dissolution medium generally leads to a reduction of the effective diffusion coefficient and hence results in decreased dissolution. For instance, Chang et al. increased the viscosity of their dissolution media using guar as the model macromolecule. Subsequently, dissolution rates of benzoic acid were reduced significantly. However, dissolution rates were not at all affected when adjusting the same viscosity using propylene glycols [18].

Temperature (T)

The temperature influences the drug's saturation solubility but also affects the kinematic viscosity (density of the liquid!) as well as the diffusion coefficient. Therefore, when performing dissolution experiments, temperature should be monitored carefully or preferably kept constant.

Particle morphology and surface roughness

Faster initial dissolution rates obtained by grinding or milling the drug can often be attributed to both an increase in surface area and changes in surface morphology that lead to a higher surface free energy [19, 20]. However, an increase in edges, corners defects and irregularities on the surfaces of *coarse* grade drug particles can also influence the effective hydrodynamic boundary layer δ_{HL} and hence dissolution rate [12, 21-23]. Depending on the surface roughness (R) of the drug particle, the liquid stream near to the particle surface may be turbulent even though the bulk flow remains laminar [9, 10]. Irregularities, edges, and defects increase the mass transfer in different ways according to the different kinds of hydrodynamic boundary layers generated. In the case of a turbulent boundary layer the overall surface roughness is assumed to behave hydraulically "indifferent" (i.e. does not increase mass transfer itself) if the protrusions and cavitations are fully located within the viscous sub-layer (δ_{VS}). The so-called "*allowable"* (=indifferent) dimension of such a surface roughness (R_{zul}) can be estimated using an equation originally developed for tubes and pipes ([24], § 21 d):

$$R_{zul} = 100 \cdot \frac{\nu}{U_A}$$

For $R<R_{zul}$ the surface roughness does not cause perturbances that increase mass transfer.

In contrast, in the case of a laminar hydrodynamic boundary layer the *critical* dimension of a surface roughness (R_{crit}) can be determined using the following relation:

$$R_{krit} = 15 \cdot \frac{\nu}{\sqrt{\frac{\tau}{\rho}}}$$

with

$$\sqrt{\frac{\tau}{\rho}} = 0.332 \cdot U_A^2 \cdot \sqrt{\frac{\nu}{U_A \cdot L}}$$

where τ represents the shear stress, ρ is the fluid density and ν stands for the kinematic viscosity. If $R>R_{crit}$, the effective hydrodynamic boundary layer close to the particle wall becomes turbulent even though the bulk flow still may be laminar! In contrast to R_{zul}, the *critical* dimension of a surface roughness (R_{crit}) depends on the characteristic length L of the particle surface and is about 10 times greater than (R_{zul}) ([24], § 21 d). In the case of a laminar hydrodynamic boundary Levich estimated that (R_{crit}) could be exceeded for Reynolds numbers as low as Re=20. This implicates that even very small irregularities or roughnesses on the surface of drug particles can have momentous effects on the hydrodynamic boundary layer δ_{HL} and hence on the dissolution rate [9, 25].

Flow along a particle surface can be affected either by cavitations or by protrusions. In both cases the flow pattern on the particle surface is changed and the dissolution rate may be altered due to local perturbances.

Fig. 6 and 7

These pictures are derived from lab experiments and illustrate that flow can become turbulent close to particle walls even when the bulk flow remains laminar. The turbulent vortices bore into the particle surface, magnifying cavitations and abrading protrusions, and hence accelerating the dissolution process ([10], chapter 4.3.5). However, irregularities and roughnesses on the surface of drug particles are expected to influence the effective hydrodynamic boundary layer δ_{HL} of *coarse grade* drug particles only. For example, Mithani investigated the dissolution of coarse dipyridamole (DPM) particles [26]. The dissolution rate of single DPM crystals was increased with time due to a considerable increase in surface roughness whereas the geometry of the crystals was maintained during dissolution. Particle geometry and morphology can be investigated using conventional scanning electron microscopy to predict these effects [10].

Fig. 8 and 9

The lower SEM shows a magnification (x7500) of the „smooth“ and regular surface area indicated in the upper SEM. The length of the edges of the cube was on the order of about 200-300 µm. The particle surface appeared to be smooth. Nevertheless, small “craters and hills” on the order of about 0.5-3 µm have to be taken into consideration. The observed cavitations and protrusion on the particle surfaces may cause perturbances, change the nature of the hydrodynamic boundary layer and hence increase dissolution. Furthermore, as was confirmed by these microscopic observations, small particles adhere at the surfaces of the larger particles due static charges [10]. This occurs particularly if the powder fraction is obtained by sieving the bulk powder. In this case dissolution might be biphasic. Subsequent to an initial “burst” phase, dissolution continues more slowly from the coarse grade “core” fraction [10, 27]. Thus, geometry and surface morphology appear to play a very important role in the dissolution of coarse grade drug particles.

Particle size

The particle size of poorly soluble drugs is generally of major importance for dissolution and absorption. For example, *in vitro* investigations performed with sulfonamides showed that the initial dissolution rate increased with a decrease in particle size, other dissolution conditions remaining constant [27]. Already in 1962 Atkinson and Kraml performed *in vivo* investigations and reported a two-fold enhancement in absorption of griseofulvin particles

with a four-fold increased surface area [28, 29]. Similar results were obtained for the micronization of felodipine, particle size having a profound effect on the *in vivo* dissolution and absorption [30]. Scholz et al. used a combination of infusion and oral administration of either normal saline or a 5 % glucose solution to maintain and establish “fasted” and “fed” state motility patterns, respectively. The absorption characteristics of both a micronized and a coarse fraction of the drug were subsequently studied under these two motility patterns. The dissolution of the coarse grade fraction was improved by the “fed” state hydrodynamics, as reflected in the nearly doubled extent of absorption. In contrast, micronized powder of the same chemical species showed less sensitivity to hydrodynamics as was reported from former studies ([31], [10], pp. 220 f, 235).

Particle size and effective hydrodynamic boundary layer: The mean hydrodynamic boundary layer generated on the surface of particles undergoing a dissolution process depends on the particle size and the particle size distribution. However, the thickness of the *effective* hydrodynamic boundary layer relies in an interdependent manner on the particle diameter and the flow rate at the particle surface. Considering particle sizes beyond 200 µm, mass transfer coefficients were found by Harriott to be independent of the particle size, provided that sufficient agitation was applied ([32], stirring rates exceeded 300 rpm). Below particle sizes of about 200 µm, mass transfer coefficients and dissolution were considerably influenced by both the stirring rate and the particle sizes. The observed interdependency decreased gradually with decreasing particle sizes and was no longer measurable below 15 µm. Considering a combination of particle size and hydrodynamics, and further provided that the media viscosity is unaltered, it appears that three cases have to be distinguished ([10], chapter 5.7).

- At a given stirring rate the effective hydrodynamic boundary layer is expected to be independent of particle size beyond a maximal particle size range, since the particle surface cannot bind the surrounding fluid to an infinite distance into the bulk. As a matter of course, dissolution still depends on convection.
- Since the *absolute* thickness of the effective hydrodynamic boundary layer is very small, below a particular size range minimum no hydrodynamic effects will be perceived experimentally with varying agitation. This, however, does not mean, that there would be no such influences! Further, the mechanisms of mass transfer and dissolution may change for very small particles depending on a number of factors like the fluid viscosity, the

Sherwood number (the ratio of mass diffusivity to molecular diffusivity) and the power input per unit mass of fluid.

- In between these two extremes, the *effective* hydrodynamic boundary layer depends on the combined effects of particle size *and* hydrodynamics. Talking about "borderline particle sizes" is meaningful only if all other relevant data, like the fluid viscosity, the diffusivity, the temperature and the saturation solubility of the compound, are additionally provided to characterize the hydrodynamic system.

Microparticles: Generally, micronized particles show less sensitivity to hydrodynamics compared to coarse grade material of the same chemical entity ([10], chapter 5.7 and chapter 12.3.5). Armenante postulated a different mass transfer process for what he termed "microparticles" [33]. The microparticle size range was defined in terms of the viscosity of the medium and the power input into the hydrodynamic system. The development of a boundary layer determines the mass transfer for "macroparticles" but contributes to a lesser extent to the microparticle dissolution since their behavior additionally depends on the hydrodynamics in micro-eddy regions. For very small particles (approx. diameters below about 5 µm in aqueous media) diffusion within the surface microclimate becomes predominant for mass transfer and particles behave more and more "like molecules" [34]. Subsequently, the *relative* influence of the bulk flow, expressed by the Reynolds term, decreases gradually [10], [35]. Thus, local turbulences may occur at milder hydrodynamic conditions for the micro- than for macroparticles, making them less sensitive to differences in the bulk hydrodynamics. Bisrat et. al. demonstrated that the thickness of the boundary layer increased with increase in mean volume diameter of the particles [36]. This increase was found to be less pronounced above approximately 15 µm diameter. It was also shown that the intrinsic dissolution rates of digoxin and oxazepam of particles <5 µm were not significantly affected by increased agitation intensities, while a sieve fraction of the same compounds in the range 25-35 µm was affected [31, 37]. Hariott investigated the dependence of the boundary layer thickness upon the slip velocity for different particle sizes [32]. The greater the "slip velocity", the smaller the boundary layer generated at the surface of the particle. Hariott found that the slip velocity, the relative velocity of the solid to the fluid, was negligible for very small, suspended particles. Thus bulk agitation should have relatively little influence on the dissolution rate of microparticles. However, at larger particle sizes the slip

velocity -and hence the boundary layer- becomes an important factor in the dissolution process.

II Hydrodynamics of compendial dissolution apparatus

Various dissolution test systems have been developed and several of them now enjoy compendial status in pharmacopeia, for example the reciprocating cylinder (USP apparatus 3), the flow-through apparatus (Pharm. Eur. 2002, 2.9.3) or apparatus for transdermal delivery systems like the paddle over disc. Hydrodynamic properties of these and other apparatus have been described only sparingly. The paucity of quantitative data related to hydrodynamics of pharmacopeial dissolution testers is lamentable since well controllable hydrodynamics are essential to both biopharmaceutical simulations and quality control. Here, we focus the discussion on the paddle and the basket apparatus since these are the most important and widely used for oral solid dosage forms. A brief treatise on the hydrodynamics of the flow-through apparatus completes this section.

1 Methods used for the investigation of flow patterns and flow rates

Flow patterns of hydrodynamic systems like the compendial dissolution apparatus may be *qualitatively* characterized by means of dilute dye injection (e.g. methylene blue) or by techniques using particulate materials like aluminium powders or polystyrene particles. Flow patterns may also be also visualized by taking advantage of density or pH differences within the fluid stream. The „Schlieren“ method, for instance, is based on a refraction index measurement. Hot wire anemometry is an appropriate method to *quantitatively* characterize flow rates. The flow rate is proportional to the cooling rate of a thin hot wire presented to the stream. Using laser doppler anemometry flow rates as low as 1 µm/s can be determined. This optic method is recognized as the “gold standard” since it is the most accurate available. However, the fact that the method can be used solely for transparent media can be a disadvantage. Topics like velocity measurement and flow vizualisation techniques are nicely covered by Tritton ([13], § 25.2-4).

2 Flow rate as a function of stirring rate for paddle and basket

Recently, studies were performed to quantitatively examine the hydrodynamics of the two most common *in vitro* dissolution testers. Rotational (tangential) fluid velocities were correlated to stirring rates at various positions within the dissolution vessels of the paddle and the basket apparatus by means of an ultrasound pulse echo method (UPE-method, [10, 38]). This method permits direct characterization of hydrodynamics as opposed to indirect methods such as via the dissolution characteristics of dosage forms, the results of which are subject to varying properties from batch to batch (for example, USP calibrator tablets). Furthermore, the technique can be used for non-transparent media and suspensions, making it possible to study flow rate effects on excipient-loaded formulations. In general, fluid velocities (in cm/s) for the paddle apparatus were determined to be about 8 to 10 times higher than compared to the basket at a given stirring rate (rpm). At most positions they correlated well and in a linear manner with the stirring rate for both the paddle and the basket.

Fig. 10

Fluid velocities using the basket method were determined to range between 0.3 and 5 cm/s (25 rpm to 200 rpm) and for the paddle method to range between 1.8 and 37 cm/s (25 rpm to 200 rpm)[1]. Possible applications of these fluid velocity data may include their use to forecast *in vitro* dissolution rates and profiles of pure drug compounds for the paddle test employing an appropriate mathematical scenario/formula like the combination model.

3 Flow pattern in paddle and basket

The following drawings illustrate the flow patterns for both the basket and the paddle apparatus.

Fig. 11 and 12

[1] Detailed sets of fluid velocity data for the paddle and the basket apparatus including various positions in the vessels and different volumes (500 ml, 900 ml and 1000 ml) of dissolution medium can be found in ([10], chapter 11.3).

An undertow can be observed visually in the paddle apparatus for stirring rates exceeding 125 rpm. The hydrodynamic region below the paddle, and, even more pronounced, below the basket, appears to be somehow "separated" from the region above the stirring device. Diffusion-driven exchange of dissolved mass between these two regions is unhampered but little (convective-driven) exchange of particulate material takes place. Flow rates given for the basket apparatus, however, are valid for the bulk flow only and likely do not reflect the influence of hydrodynamics on dissolution *inside the basket*. Nevertheless, vessel hydrodynamics of regions *outside the basket* may be relevant for dissolution of solid formulations with respect to fractions of particulate material that have fallen though the basket screen. Further, hydrodynamics inside the basket may also be influenced by the "outside" bulk hydrodynamics and the stirring rate in a way that, starting with a rotational speed of about 100 rpm or more, contact between the bulk fluid and the formulation inside the basket becomes restricted. At these rates the basket may be regarded as a "closed container" with limited access to "fresh" dissolution medium and less turbulent flow conditions. For some specific purposes, the basket could even be used to serve as a "rotating cylinder" with the formulation placed outside the basket at the bottom of the vessel. Such a modified apparatus could be advantageous when mild but reproducible hydrodynamic conditions are desired.

4 Fluid velocities at various positions and volumes

Rotational flow below the stirring device

Fluid velocities for the rotational (tangential) flow below the stirring device employing 900 ml of medium were determined to be 8.5 cm/s at 50 rpm and 16 cm/s at 100 rpm, the most widely used agitation rates in the paddle apparatus [10]. The fluid velocities for the rotational flow measured at various (lateral) positions of the dissolution vessels do *not* differ significantly. This is true for the basket as well and indicates that the fluid is homogeneously accelerated within the vessel [10].

Vertical flow below the stirring device

Hydrodynamics at the bottom of the vessel (position U) is of particular interest since a lot of non-floating tablet and (soft gelatin, primarily) capsule formulations remain there after disintegration and throughout the dissolution test and are therefore primarily exposed to this

hydrodynamic flow regime. “Coning effects” are sometimes observed at low stirring rates in the paddle apparatus at about 50 rpm at the bottom of the hemispheric vessel. This undesired phenomenon preferably occurs employing disintegrating type tablets with high loads of insoluble, dense excipients. There is no simple linear correlation between the stirring rate and the *vertical* (axial) flow rate (upward stream) at the bottom of the vessel. The vertical flow rates at the bottom region of the vessel are very low (< 1.5 cm/s). An insufficient upward stream in combination with a far stronger rotational (horizontal, tangential) flow might explain the observed „coning effects“.

Fig. 13

Vertical flow above the stirring device

Close to the wall of the dissolution vessel (position O1) the flow is directed upwards, creeping along the wall as indicated by a negative algebraic sign (figure not shown). For the basket this is also true in position O2 indicating an upward directed stream for the bulk flow above the basket whereas for the paddle an undertow is recorded at position O2 (positive algebraic sign).

Fig. 14

Fluid velocities employing different volumes

The lower the volume of medium employed in a dissolution test, the higher are the flow rates *ceteris paribus*. A test volume of 500 ml results in a considerable increase in the fluid velocities at any given stirring rate compared to 900 ml of dissolution medium. There appears to exist a significant mass/volume effect on hydrodynamics. Up to the level of the paddle, for example, the rotational (tangential) fluid velocity at 100 rpm was determined to be 16.8 cm/s using 900 ml of dissolution medium compared with 20.5 cm/s employing a volume of just 500 ml [10]. The undertow generated at the bottom of the dissolution vessel, where the formulations are often located during the tests, was also found to be higher using 500 ml than 900 ml. Thus, the volume used in the dissolution tests cannot be ignored and has an influence not only in terms of the concentration driving force for dissolution but also from an hydrodynamic point of view ([10], chapter 11.3.3 and Fig. 11.10 page 185). Therefore, special care has to be taken in the method validation for quality control purposes when

changing the volumes, e.g. when the method is adapted for a higher strength dosage form. This statement also holds for the basket.

Fig. 15

5 Prediction of fluid velocities for the paddle and the basket

The empirically gained knowledge of the fluid velocities in the dissolution vessels at rotational speeds from 25 rpm to 200 rpm resulted in a number of parameters that found application in developing equations to correlate stirring rates and flow rates (tangential fluid velocities) at specific regions within the vessel. Flow rates (U_A) in the paddle and the basket apparatus can be calculated for any desired stirring rate (ω) by means of a simple linear relationship using the data for the parameters b[1] and b[0] reported in [10, 38].

$U_A = b[1]*(\omega)+b[0]$

U_A is given in (cm/s), ω in (1/min.). Two examples illustrate the applicability of this relationship:

(1) The fluid velocity approximately 1 cm below the paddle (position S1) at a stirring rate of 110 rpm employing 900 ml of dissolution medium was calculated to be 17.98 cm/s. Indeed, at 100 rpm the flow rate was determined to be 16.01 cm/s using the UPE method, and at 125 rpm the flow rate was measured to be 20.29 cm/s, both of which give some plausibility to the calculated value.

(2) The bulk flow rate up to the mark of the basket (position S2) employing 60 rpm and 500 ml of dissolution medium, for instance, was calculated to be 1.5 cm/s. Comparison to experimental data verified the concept: 1.17 cm/s were obtained for 50 rpm and 1.97 cm/s for 75 rpm, respectively. [10].

Rotational fluid velocities are calculated since horizontal (rotational) flow prevails in the hydrodynamic regime within the dissolution vessels. Thus, the overall hydrodynamics and hence dissolution is dominated by the substantially higher rotational (tangential) fluid velocities.

6 Reynolds numbers *in vitro*

Bulk Reynolds numbers

In the paddle method, *bulk* Reynolds numbers range from Re=2292 (25 rpm, 900 ml) up to Re=31025 (200 rpm, 500 ml). In contrast, Reynolds numbers employing the basket apparatus range from Re=231 to Re=4541. These Reynolds numbers are derived from dissolution experiments in which oxygen was the solute ([10], chapter 13.4.8) and illustrate that turbulent flow patterns may occur within the *bulk* medium, namely for flow close to the liquid surface of the dissolution medium. The numbers are valid provided that the whole liquid surface rotates. According to Levich, the onset of turbulent bulk flow under these conditions can then be assumed at Re~1500 [9].

Particle-liquid Reynolds numbers

As mentioned earlier, Reynolds numbers determined for the bulk flow have to be discerned from Reynolds numbers characterizing a particle-liquid dissolution system. The latter were calculated for drug particles of different sizes using the Reynolds term according to the combination model. The kinematic viscosity of the dissolution medium at 37 °C is about $7x10^{-03}$ cm^2/s. The fluid velocities (U_A) employing the paddle method at stirring rates of 50 to 150 rpm can be taken from the literature and may arbitrarily be used as the slip velocities at the particle surfaces. Based on these data, particle-liquid Reynolds numbers were calculated to range from Re=25 (50 rpm) to Re=90 (150 rpm) for coarse grade particles with a median diameter of 236 µm. In contrast, Reynolds numbers for a batch of micronized powder of the same chemical entity with a median diameter of 3 µm were calculated to be significantly lower (Re<1) indicating less sensitivity towards convective hydrodynamics ([10], chapter 12.3.8). Based on the aforementioned considerations for spheres, bulk Reynolds numbers of about Re>50 appear to be sufficient to produce the laminar-turbulent transition around a rough drug particle of coarse grade dimensions.

7 Hydrodynamics of the flow through apparatus

The flow-through cell system (USP apparatus 4) is described under the monograph <724> dealing with “drug release” and is becoming more important for the dissolution of solid oral dosage forms. Standard flow rates of 4, 8 and 16 ml/min. are prescribed and a sinusoidal flow profile is provided having a pulsation rate of 120±10 pulses per minute. Cammarn and Sakr

used an alternate approach to describe hydrodynamics and dissolution performance of the flow through cell system involving dimensionless analysis [39]. Volumetric flow rates up to 53 ml/min were employed in these tests. These values corresponded to linear fluid velocities of less than 2.3 cm/s. Reynolds numbers were calculated under these conditions to range from 7 to 292 indicating that bulk flow is laminar. For example, a Re=16.3 was determined for a flow rate of 10.4 ml/min (12 mm cell, single vertical). Dissolution rates were determined to be a function of media linear velocity (in cm/s) rather than being described by volumetric flow rate. Tablet diameter, shape and surface were found to be critical to dissolution rate of e.g. non-disintegrating tablets.

III *In vivo* hydrodynamics, dissolution and drug absorption

Absorption of orally administered drugs depends mainly on dissolution if the compound is poorly soluble but highly permeable. A variety of factors can influence *in vivo* dissolution, such as the properties of the drug itself (polymorphism, pKa, complexation behavior, diffusivity), the formulation variables (capsule shell, tablet hardness, particle size distribution of excipients), the composition of the gastrointestinal fluids (pH, buffer capacity, solubilisation and wettability properties) and -last but not least- the hydrodynamics of the gastrointestinal tract. Many poorly soluble drugs fail to be completely bioavailable after oral dosing. In the case of dissolution rate limited absorption the thickness of the boundary layer can influence the dissolution. The thickness of the boundary layer is, in turn, dependent upon the (*in vivo*) hydrodynamics. *In vivo* hydrodynamics, however, depend on gastrointestinal *motility.* Although much is known about motility patterns, little is known about the relationship of motility patterns and gastrointestinal *hydrodynamics.* To the best of our knowledge it is not yet clear in which way exactly and to which extent gastrointestinal motility correlates with intestinal flow rates, how fast the liquids progress and which flow rates are produced in the gut by the different motility patterns. According to Johnson et al. (1997) the *velocity* of propulsive contractions in the upper small intestine seems to be the major determinant of intestinal transit [40]. Nevertheless, two important issues remain partially unresolved:

1. So far we are not able to define or predict intestinal flow rates solely based on the knowledge of motility data.

2. It is still challenging to isolate hydrodynamic influences on drug dissolution *in vivo* from other factors that can play a role in absorption.

1 Gastrointestinal motility

In the gastrointestinal tract different hydrodynamic conditions are present, depending on the fasted or the fed state. Contraction patterns are controlled in terms of electromechanical impulses (myoelectric activity) as well as by various hormones (CCK, secretin, glucagon, motilin and insulin, for example). In the fasted state the motility pattern is regulated by the (interdigestive) migrating motor complex ((I)MMC), a cyclic pattern consisting of mainly three phases (I, II and III in that order) with a duration of approximately 90-120 min. IMMC starts at the proximal GI tract (lower oesophagus, stomach and proximal duodenum). During phase I (approx. 45-60 min), residence times are long but there is barely any fluid movement since there are no contractions. In phase III, lasting about 10 min and followed by a "quiescent phase" of about 0-5 min, all "slow waves" (rhythmic fluctuations of the cellular membrane potential) are associated with "spikes". As a result, about half of the contractions propagate the GI contents up to 30-40 cm aborally and fluid movement is so rapid that often there might be insufficient time for dissolution to occur prior to reaching the absorptive sites. In contrast, phase II conditions, with a duration of 30-45 min, are most likely to favor drug dissolution. This IMMC phase is most similar to a postprandial status in terms of the percent of slow waves associated with spikes, distribution between segmental and propagated contractions and distances over which peristaltic waves are propagated.

The motility pattern of the fed state is more regular. Sixty-five percent of propagated contractions travel only 3-9 cm. There is sufficient chyme present in the gut lumen to serve as the dissolution medium and the chyme is more or less in continuous movement. Due to the rhythmic segmentation contractions, a more frequent local acceleration of the chyme can be assumed. It is likely that the rate and the frequency (but not necessarily the type) of the bulk flow is different in the fed than in the fasted state and that this could lead to changes in dissolution, dependent on the sensitivity of the formulation. Taking these physiological variations into consideration, the dissolution of poorly soluble drugs and the release from formulations sensitive to hydrodynamic changes is expected to be more effective in the fed than the fasted state.

2 Gastrointestinal hydrodynamics

Hydrodynamics of the upper gastrointestinal tract are characterized by (1) the kinetics of gastric emptying and (2) by the small intestinal transit and the flow rate of intestinal fluid (chyme). Gastric emptying becomes important for the overall absorption of certain drugs because it can act as the "gate keeper" controlling delivery of drugs to the absorptive sites in the intestines. This is of particular importance for drugs that are highly soluble in gastric juice like furosemide, acetaminophen, aspirin, lidocaine or amoxicillin, to name but a few examples. Bioavailability of these compounds is limited by the time required for them to reach the absorptive sites in the duodenum, jejunum and ileum, a time which is primarily controlled by gastric emptying. In the case of poorly soluble but highly permeable drugs, both the flow rate *and* the composition and volume of chyme available for dissolution are the predominant factors. Flow rate and volume are both of importance since they can influence intestinal transit and the time available for *in vivo* dissolution as well as the time available for contact of the dissolved drug with the absorptive sites.

3 Gastric emptying

Gastrointestinal transit of formulations including solid pharmaceuticals and multiparticulate dosage forms is covered by Clive Wilson et al. (chapter 7). Therefore, the focus of the discussion here is on the hydrodynamics of gastric emptying and small intestinal transit of liquids. The volume, the temperature and the composition (caloric content, osmolality, pH, viscosity) of gastric contents influence gastric emptying. Among these factors, caloric content is most important for the regulation of gastric emptying kinetics of liquids.

Non-caloric liquids

The emptying of isotonic non-caloric fluids is proportional to the initial volume and the distension of the stomach. Quantities of about 600 ml most likely activate barostatic receptors. Gastric emptying of small volumes of non-caloric (non-nutrient) fluids correlates with the corresponding phase of the antral „Interdigestive Migrating Myoelectric Complex" (IMMC) in humans. During phase I gastric emptying is negligible whereas it reaches maximum during phase III. Although gastric emptying of volumes < 50 ml is highly dependent on the motility phase, this is not so true for larger volumes (> 200 ml), as demonstrated by Oberle [41]. First order kinetics tend to apply for volumes of about 200 ml

or larger. Using the canine model it has been shown that volumes bigger than 300 ml establish fed state like conditions. However, if the viscosity of the liquid is elevated, this induction can happen at lower volumes. Further, the emptying of viscous liquids is considerably slower compared to non-viscous liquids of the same volume [42, 43]. The half-life of gastric emptying ($GE_{50\%}$) of non-nutrient liquids ranges from 12 min. (200 ml administered) to 22 min. (50 ml administered)[2]. In general, gastric emptying of non-caloric liquids is much faster than for caloric fluids.

Caloric liquids

The rate of delivery of calories to the duodenum is kept within a very narrow range, regardless of whether the calories are presented as carbohydrate, protein, fat, or as a mixed meal. Caloric liquids of volumes greater than 200 ml empty slower than non-nutrient liquids of identical volume. The energy content of the liquid is the most important determinant of the rate of gastric emptying and half-life ($GE_{50\%}$) and this determinant is regulated mainly in the duodenum. Glucose solutions (400 ml, orally administered) have been found to obey linear release kinetics and to empty at an average rate of 2.1 kcal/min. regardless of concentration given. [44]. McHugh et al. were the first to report calorie-driven, linear emptying of orally administered glucose solutions with a constant rate of 0.4 kcal/min. for *macaca mulatta* [45, 46]. The authors demonstrated that half-life of gastric emptying doubles for a given volume if the caloric density of the fluid administered is doubled. Thus, caloric fluids are emptied in a manner which presents a constant caloric delivery to the duodenum regardless of the glucose concentration. This rate is, however, species dependent. Neither motility phase I nor motility phase II of the IMMC has any significant impact on the gastric emptying rate of the glucose solutions [47].

Non-linear initial release kinetics for caloric fluids

The larger the load of glucose delivered to the duodenum, the longer and more complete is the inhibition of gastric emptying. However, gastric emptying is not a continuous process. Rather the stomach *initially* empties even a nutrient solution rapidly as though it was saline. Hunt et al. administered 1134 polycose meals of different energy contents (0.5 to 2.0 kcal/ml) and various volumes (300, 400 and 600 ml) to 21 subjects [48]. The mean rate of the calories delivered to the duodenum was found to be 2.5 kcal/min. confirming previous results of

[2] see [10], chapter 15.1.2, for a detailed synopsis including original references

Brener et al. (1983) [44]. However, for the greater volumes (400 and 600 ml, respectively) the rate of calorie emptying was increased during the initial 30 min. up to 3.3 and 4.0 kcal/min. revealing non-linear initial kinetics. Calbet et al. (1997) described exponential release kinetics characterizing the *initial* phase of gastric emptying of 600 ml of glucose solution 2.5 % [49]. Schirra et al. (1996) additionally reported non-linear kinetics for human gastric emptying of concentrated glucose solutions (400 ml, 12.5 and 25 % (w/v) [47]). Thus, gastric emptying of caloric fluids is obviously of a biphasic nature. The short initial phase is dominated by first order kinetics and followed by a linear, steady-state release of the remaining fluid. Gastric contents have to reach the duodenal (and ileal) glucose receptors before „feedback" mechanisms are fully activated. The time gap between the administration of the caloric fluid and the subsequent activation of gastrointestinal „feedback" mechanisms plays a role in this behavior. Half-lives ($GE_{50\%}$) of gastric emptying were found to range from 49 min. (500 ml glucose 10%) to 118 min. (500 ml glucose 25%) and from 23 min. (200 ml glucose 25%) to 94 min. (400 ml glucose 25%). A detailed synopsis of human gastric emptying data including kinetics and release rates of various nutrient solutions have been summarized by Diebold ([10], chapter 15.1.2). The delay in gastric emptying resulting from ingestion of proteins, lipids or carbohydrates is similar to those summarized here, provided that the energy content is the same, with an emptying rate of about 2 kcal/min.

Interspecies differences

A rank order of gastric emptying ($GE_{50\%}$) exists among species. Gastric emptying rates for monkeys (*macaca mulatta*) and dog, which are considered comparable, are slowest. Corresponding values for humans are slightly higher whereas porcine gastric emptying is much faster ([10], Tab.15.6).

Osmolality

The influence of osmolality on gastric emptying appears to be of minor importance for liquids [49] [50]. However, employing hyperosmotic saline solutions (500 ml) half-life of gastric emptying was demonstrated to increase from 4.9-13.8 min. (isoosmotic) up to 53.1 min. (hyperosmotic) [51]. The further the liquid deviates from isoosmotic, the slower will be its rate of emptying. Thus, hypotonic and hypertonic fluids empty more slowly than do isotonic fluids. It has been shown that the "osmoreceptor" for the feedback signal resides in the duodenum. So long as duodenal contents are kept isotonic, gastric emptying of non-

caloric fluids is rapid. There is no negative feedback to slow gastric emptying when hypertonic fluids are placed directly into the jejunum. The nature of this feedback mechanism for inhibiting gastric emptying has not been elucidated but presumably is both neural and humoral in nature. The caloric load of ingested meals and liquids predominates the influence of osmolality on gastric emptying in the fed state [50].

pH

The lower the pH, the slower is gastric emptying. Secretin presumably modulates this effect since acid in the duodenum is the prime stimulus for its release and secretin has been shown to delay gastric emptying. In addition, neural receptors that respond to acid are present in the duodenum.

Liquid-solid meals

If the *per os* meal consists of liquid *and* solid components, gastric emptying exhibits a biphasic mechanism with the exception of emptying of solid particles in MMC phase III, gastric emptying of solids into the duodenum takes place only if these particles are smaller than 1-3 mm in diameter [43, 52]. These particles are emptied, after a short lag phase, according to linear kinetics whereas the liquid fraction often exhibits an exponential or a biphasic-(exponential) release kinetics [53-55].

Variability of gastric emptying

Gastrointestinal flow rates in the upper small intestine were demonstrated to be highly variable following oral administration of both saline 0.9 % and glucose solution 20 % [10].

Fig. 16

The observed variability was more pronounced for the saline than for the glucose solution and was attributed mainly to the influence of gastric emptying rather than to MMC driven transit variations [10]. Variability of gastric emptying due to antral motility (typical of phase III contractions) and subsequent non-uniform gastric emptying can cause double peaks in the absorptive phase of concentration versus time plots and can be seen with solids, suspensions and solutions. This was demonstrated e.g. for the absorption of cimetidine following oral administration in the fasted state in humans. [56].

4 Intestinal transit

Sma1l intestina1 transit time represents 10-25 % of the tota1 GI residence time and usua1ly takes between 2 and 5 h. Compared to transit through the large intestine, the overall small intestinal transit is shorter, varies less and is more important for the absorption of both nutrients and drugs. Intestinal transit rate of fluids within a particular segment of the upper small intestine depends on fasted *versus* fed state and, in the fasted states, on the phase of the MMC in the particular segment at the time of observation. Under physiological conditions the chyme moves aborally but short periods of retropulsion and „gushes" can occur intermittently. Propulsion of chyme is fastest in the duodenum and slowest in the ileum. It can be influenced by age, pregnancy, gender or by certain diseases, although small intestinal transit is generally less sensitive to these influences than large intestinal transit. Small intestinal transit can be accelerated artificially by co-administration of certain prokinetic drugs like metoclopramide, bromopride or domperidone and slowed down by inhibitors like loperamide and opioids or by anticholinergics, such as ipratropiumbromide, tropicamide or trihexiphenidyl. The increase of the transit time is linked to an increase in time available for dissolution. On the other hand, motility-inducing agents, such as cisapride, which affects the small intestine as well as the colon, increase propagative contractions and hence may favour drug dissolution although limiting contact time of the dissolved drug with the absorptive sites.

Transit rates and flow rates in the human small intestine

Mean and median transit rates of liquids passing the upper small intestine employing different techniques and various liquid meals were determined to range between 1 and 4.8 cm/min. (see [10], Tab. 15.14 for a synopsis). Investigations on this subject were performed by [57-62], [63]. Jejunal and ileal flow rates in the human midgut range between 1 and 4.5 ml/min. (see [10], Tab.15.13 for a synopsis). Dillard et al. (1965) reported 15 ml/min.. However, these authors employed high perfusion rates of about 14 ml/min. [64]. Kerlin et al. (1982) performed flow rate measurements on intestinal segments of about 20 cm. They used an aspiration method employing phenol red (PSP) at a perfusion rate of 1 ml/min. [65]. However, it seems questionable if such short distances are representative for the hydrodynamics of the small intestine in general. Jejunal flow rates are found to be greater

than ileal flow rates as was confirmed by Johnson et al. (1997) for the *relationship* of jejunal and ileal transit rates in the *canine* upper intestine [40].

Tab. 1

Jejunal and ileal flow rates are somewhat higher in the fed state than in the fasted state as demonstrated by several authors [65-67].

Influence of osmolality on intestinal transit and on chyme volume available for dissolution

There is clear evidence that *in vivo* hydrodynamics, namely mean intestinal fluid transit, depends on the osmotic conditions within the small intestine. Trendelenburg was the first author to perform systematic research on this subject - in 1917 [68]. Holgate and Read [69] found that the intestinal transit rate was increased by hyperosmotic Mg-sulfate solutions despite the retardation of gastric emptying. Miller and co-workers reported oro-caecal transit times of intestinal chyme being significantly reduced from 205 min. to 35 min. (Median, $P < 0.01$) by coadministered lactulose (10 g per 300 ml standard meal, [70]). The authors concluded that intestinal transit was accelerated due to massive secretion of water into the lumen of the small intestine. Sellin and Hart (1992) administered 250 ml of glucose solution 20 %. Mean oro-caecal transit times were significantly decreased due to the hyperosmolality of the fluids [71]. Similar observations have been reported using the canine model. Transit rates in the canine upper small intestine were significantly different after oral administration of hyperosmotic glucose solution (20 %, 200 ml) compared to the same volume of 0.9 % sodium chloride solution (2.7 cm/min. versus 1.1 cm/min., n=8, $P<0.001$, bifactorial ANOVA) [10]. Ingestion of hypertonic liquids stimulated net water efflux across the intestinal wall into the GI lumen, possibly increased intestinal peristalsis and accelerated the fluid transit *even though* gastric emptying was retarded. Apart from an acceleration of fluid transit the increase of volume in the small intestine causes a considerable increase of *in vivo* dissolution of poorly soluble drugs as was demonstrated with the use of an invasive aspiration method ([10], chapter 16). The (cumulative) dissolved (not absorbed) fraction of felodipine (F_{CDNA}) correlated well with the recovered volume at mid-jejeunum of labradors. ($R=0.972$, Pearson and Bravais, $P<0.001$). The more liquid/chyme was available in the gut lumen, the faster was the *in vivo* dissolution. This result is in compliance with the equations adapted from Noyes, Whitney, Nernst and Brunner.

Fig. 17

Transit rates and flow rates at canine small intestine

Due to the paucity of data for humans, it might be helpful to look on the canine model. In general, mean intestinal transit and flow rates of the dog correspond well to analogous data from humans. Flow rates at the canine *jejunum* after administration of 200 to 600 ml of various liquid meals ranged between 1 to 4 ml/min. and sometimes up to 7 ml/min. [72-76]. Further, intestinal flow rates are highest in Phase II/III of the MMC, followed by postprandial flow rates. Flow rates in the canine duodenum and the proximal jejunum after administration of various liquids range between 2 and 13 ml/min. [30, 43, 77]. For instance, median *duodeno-jejunal* flow rates were determined to be 8.3 ml/min. after oral administration of 200 ml glucose solution 20% [10]. These flow rates obtained following the administration of glucose solutions is in good agreement with previous data of Brener et al. for humans [44]. They reported a gastric emptying rate of 2.13 kcal/min, which corresponds to a theoretical flow rate of about 10 ml/min.. However, mean flow rates occurring in the human upper small intestine often appear to be somewhat lower than in the canine small intestine [41].

Variability of intestinal transit and gastrointestinal flow rates

Considering the limited bioavailability of many poorly soluble drugs, any variability of gastrointestinal flow or transit in the small intestine could have a pronounced influence on *in vivo* dissolution and absorption. Intestinal transit of liquids was shown to be variable both inter-individually and intra-individually. Caride et al. (1984) compared a scintigraphic method to determine gastro-caecal transit times with the „hydrogen breath technique" [61]. Nineteen study participants received isotonic lactulose solution and 99^{m}-Tc-DTPA. Mean gastro-caecal transit times (MTT) were found to be comparable for both experimental techniques (mean about 75 min.±8 min.). However, individual transit times exhibited a relatively broad range, from 31 to 139 min.. Cobden et al. (1983) found inter-individual transit times to range from 25 to 150 min. in a study with 21 participants [60]. The authors employed the „hydrogen breath technique" and administered 200 ml of 10 % lactulose orally as the test solution. "Gushes", anterograde and retrograde directed fluid propulsions in the upper small intestine, constitute another prominent source of variability. These produce extremely high flow rates, particularly close to the pylorus, but these "flow peaks" are of

short distance and duration [57, 78]. Therefore, they are unlikely to favour intestinal dissolution. The same is true for the transpyloric flow of non-caloric liquids from the stomach, which is not a continuous process but rather is linked to pyloric contractions and occurs in short episodes of 1 to 3 sec. about three times a minute [79].

5 Techniques used for the investigation of gastrointestinal hydrodynamics

There are a number of experimental methods and techniques used for the investigation of gastrointestinal hydrodynamics in humans. An introduction to this subject including the intubation method, gamma scintigraphy, radiotelemetry and the hydrogen breath technique can be found in Macheras et al. ([80], chapter 5.3.6). Aspiration techniques and gamma scintigraphy are the most common methods used for the investigation of *in vivo* hydrodynamics of liquids. Of these two, scintigraphic experiments are less invasive. The dosage form (or a liquid carrier) is labelled with a gamma emitter (usually ^{99m}Tc or ^{111m}In). The transit is then followed by a gamma sensitive sensor or camera. Gastric emptying times and small intestinal transit rates can be selectively investigated within the course of the same experiment. This permits separation of any interdependencies of intestinal transit and gastric emptying [10]. In contrast to most aspiration methods, the phases of gastric motility are not interrupted, e.g. by frequent intubation, since no fluid must be aspirated. Thus, duodeno-jejunal and ileal feedback mechanisms remain intact and can influence gastric emptying in a physiological manner. On the other hand, comparability to flow rate data already in literature is often limited - a common disadvantage of most scintigraphic methods. Moreover, Beckers et al. found that scintigraphic techniques generate gastric emptying data that are up to 70 % higher than those from aspiration experiments for methodical reasons [81, 82]. The authors found human gastric emptying half-lives ranging from 150 to 200 min. (600 ml, 444 kcal). Another disadvantage of this method is that the drug itself cannot usually be labelled because carbon, nitrogen and oxygen radionuclides are positron emitters with very small ha1f-lives and high radiation burdens. A further limitation to this technique is that it cannot distinguish between a radionuclide present as a solid from one in solution.

6 Reynolds numbers in the upper small intestine

The overall situation *in vivo* is far more complicated than the hydrodynamics in dissolution apparatus. Moreover, only a few data are available to exactly characterize the flow rate and the transit rate for the different segments, motility patterns and prandial states of the human small intestine. Therefore, it is a challenge to calculate meaningful and valid Reynolds numbers for the hydrodynamics of the small intestine.

Reynolds number for bulk flow

The Reynolds number characterizing laminar-turbulent transition for *bulk* flow in a pipe is about Re~2300 provided that the fluid moves uni-directionally, the pipe walls are even and behave hydraulically smooth and the internal diameter remains constant. However, intestinal walls do not fulfill these hydraulic criteria due to the presence of curvatures, villi and folds of mucous membrane, which are up to 8 mm in the duodenum, for instance. Furthermore, the internal diameter of the small intestine is estimated to be about 3 to 4 cm and does not remain constant. Not only does the diameter decrease with increasing distance from the pylorus, but the gut wall contracts, leading to momentary fluctuations in diameter.

Fig. 18

Nevertheless, *approximate* bulk Reynolds numbers may be calculated using a kinematic viscosity of (ν) =7x10^{-3} cm^2/s (water, 37 °C) for intestinal chyme and an internal diameter of the small intestine of 3 cm. Employing jejunal flow rates of 0.5 to 4.5 ml/min. bulk Reynolds numbers of Re~0.5 to Re~4.5 are then obtained. As previously demonstrated, median flow rates of 35 ml/min., including (short period) "spike" flows beyond 100 ml/min.[3], can occur at midgut after administration of non-nutrient liquids [10]. But even taking into account such extremely high flow rates, bulk Reynolds numbers of 35<Re<100-125 are obtained. Thus, *bulk* flow at midgut is unlikely to be turbulent for considerable periods of time. This can be chiefly attributed to the relatively low flow rates and the somewhat elevated viscosity of the intestinal fluids. It would take consistently higher flow rates in both, the fed and the fasted state, to permanently induce turbulence in the chyme flow of the human small intestine.

[3] This apparently high flow rate may be an artefact of the canine experiments, in which removal of the fluids at mid-jejunum through a fistula may have eliminated *long-range* feedback inhibition of flow.

However, perturbances may occasionally occur close to the intestinal wall due to folds, villi and curvatures.

Particle-liquid Reynolds number

The diameter of drug particles and hence the surface specific length L is much smaller than the pipe diameter. For this reason particle-liquid Reynolds numbers characterizing the flow at the particle surface are considerably lower than the corresponding bulk Reynolds numbers. *Particle-liquid* Reynolds numbers for particle sizes below 250 µm were calculated to be below Re~1 for flow rates up to 100 ml/min.. However, this circumstance does not limit the applicability of the boundary layer concept since in aqueous hydrodynamic systems the Peclet number (Pe) is still greater than 1 ([9, 10], chapter 5.1 and 12.3.8). Furthermore, the surface of a drug particle is far from being smooth and even. Craters and protrusions may cause perturbances at the particle surface and elevate the corresponding Reynolds numbers so that the particle surface may experience turbulent conditions *even though* the bulk flow is laminar. Moreover, the shape of the particles differs more or less according to the origin of the fraction (grinded, sieved, precipitated). Above all, Stokes law of creeping (bulk) flow can be used for smooth spheres only if Re<0.5 ! Thus, in the case of "rough" drug particles, Re~0.5 might be an appropriate magnitude to characterize the laminar-turbulent transition for flow around a sphere. Ground or milled drug particles, with more defects, protrusions and rough surfaces, can be reasonably expected to produce laminar-turbulent transition at much lower Reynolds numbers, e.g. in the range of 10^{-2}<Re<1. Thus, although neither fed state nor fasted state flows are likely to provoke a laminar-turbulent transition for the *bulk flow,* the drug *particle* potentially "sees" a turbulent flow pattern at physiological flow rates, since the crucial particle-liquid Reynolds number for the laminar-turbulent transition at a rough, edged and spherical particle surface is about $Re_{crit} \leq 0.5$.

In vitro-in vivo comparison of Reynolds numbers

Reynolds numbers calculated for the *in vivo* hydrodynamics are considerably lower than compared to the corresponding *in vitro* numbers, both for bulk and particle-liquid Reynolds numbers. Remarkably, *bulk* Reynolds numbers *in vivo* appear to have about the same magnitude as *particle-liquid* Reynolds numbers characterizing the flow at the particle surface *in vitro* using the *paddle* apparatus. In other words: It appears that hydrodynamics *per se* play a relatively minor role *in vivo* compared to the *in vitro* dissolution. This can be attributed to

physiological co-factors that greatly affect the overall dissolution *in vivo* but are not important *in vitro* (e.g. absorption and secretion processes, change of MMC phases, complex composition of chyme, bile acids, mucus and further components). These influences may sometimes overrule hydrodynamic effects *in vivo* and make it difficult to selectively measure any hydrodynamic effects on *in vivo* dissolution.

7 Intestinal hydrodynamics can influence absorption

Intestinal transit and absorption of nutrients

The purpose of the fasting motor pattern is to keep the small intestine swept clean of bacteria, undigestible meal residua, desquamated cells, and secretions. In contrast, the purpose of the fed pattern is to produce thorough mixing of the chyme with the digestive enzymes and provide maximal contact between the absorbing cells and the intestinal chyme. Thus, absorption is greatest during the fed motor pattern even though the motility is lower in terms of transit rate than in MMC phase III. For example, glucose, water and electrolytes are considerably better absorbed from isolated canine gut in the fed than in the fasted state motility pattern, owing to a significant reduction of the small intestinal transit [83]. Segmental contractions over distances of 1-4 cm encourage mixing of the lumenal contents in the fed state, leading for example to better digestion of 0.5 and 2 mm liver particles in the fed state [84]. Apart from the fed state composition of chyme, the transit rate and segmental contractions associated with an increase in mixing efficiency, absorption depends on the volume of chyme available for dissolution. Not only do the ingested food and fluids directly influence the volume in the upper GI tract, they also stimulate secretion of gastric acid, bile and pancreatic juice.

Intestinal transit and drug absorption

GI absorption of many poorly soluble drugs depends on small intestinal transit as demonstrated for ketoprofen, nifedipine, haloperidol, miconazole and others. Small intestina1 transit rate and transit time become important factors in drug absorption particularly when the ratio of dose to solubility is high and dissolution rate is very slow or when the drug is taken up selectively at a specific location of the intestine („absorption window“). In this case the extent of absorption is limited by the residence time at the uptake sites, as in the case of lithium carbonate, which is taken up by the sma1l intestine but not by the colon. For drugs

that are highly soluble in gastric juice, like atenolol for instance, no influence on the absorption was observed when intestinal transit rate was reduced about 50 % by co-administration of codeine phosphate [91]. In contrast, depending on particle size, hydrodynamics can influence drug absorption of *poorly soluble* drugs as demonstrated in pharmacokinetic studies of felodipine with fistulated Labradors [30]. The hydrodynamic influence on the bioavailability of felodipine (aqueous solubility: 1.2 µg/ml at 37°C, log P 4.5 for toluol/water) was selectively investigated and revealed a dependency of the hydrodynamic effect on the particle size *in vivo*. A twofold higher bioavailability after administration of a felodipine suspension under hydrodynamic conditions representative of the fed state compared to the fasted state was observed for the coarse grade compound. In contrast, no change in the bioavailability with hydrodynamic conditions was observed for micronized drug. The coarse grade particles appeared to be more sensitive to hydrodynamics than the micronized [10, 31, 36]. *In vivo*, however, the particle size itself appears to have a more important influence on bioavailability than the hydrodynamics *per se*. Subsequently, improved absorption attributed to the reduced particle size often overrules the influence of altered hydrodynamics although the latter affects dissolution, too.

Fig. 19

"Levelling" of in vivo hydrodynamics?

Often, no overt influence of gastrointestinal hydrodynamics on the absorption of drugs is observable *in vivo*. Therefore, one may ask, which role do gastrointestinal hydrodynamics play in relation to other physiological factors relevant to the absorption of drugs? Arguing in a more teleologic and speculative way one must point out that the gastrointestinal tract of mammalians was surely not designed for the gastrointestinal absorption of drugs but primarily optimized for food uptake and exploitation of nutritional components. Evolution had to take care of an efficient transport, digestion and absorption system for nutritional substrates of all kinds and provenience. Thus, it might have been advantageous if the species was able to efficiently absorb *small quantities* of food, exploit *different sources* of food (various plants and animals) and to cope with varying nutritional components (fats, carbohydrates, peptides….), regardless of their availability and relative proportions. Adapted omnivores like primates may have had some benefit compared to „specialists" like carnivores or vegetarians since good times can change for animals in nature over short time-spans as

well as on an evolutionary time-scale. Intestinal hydrodynamics that are extremely sensitive to different “input variables” would also have been vulnerable to environmental changes. For sure, this would not have been conducive to efficient absorption nor to nutritional supply and might have been a permanent source of malabsorption leading to crucial negative selection. These considerations may perhaps explain the “levelling” of GI hydrodynamics in the light of evolution.

8 Representation of gastrointestinal motility patterns and flow rates by in vitro hydrodynamic conditions

Abrahamsson et al. demonstrated that human intestinal hydrodynamics were reflected *in vitro* using the paddle method at stirring rates of about 140 rpm ([85], paper V). The author used erosion sensitive HPMC matrix tablets containing a poorly soluble, neutral and lipophilic ingredient. The formulations were susceptible to mechanical stress. However, human studies to establish such correlations are expensive and time consuming. As the anatomy and the physiology of the gastrointestinal tract of labradors resembles the human GI tract, this canine breed can serve as a model to simulate human intestinal hydrodynamics. Preliminary results indicate, that, following oral dosing of micronized felodipine powder under hydrodynamic conditions representative of the fed state canine intestinal hydrodynamics were reflected *in vitro* employing the paddle method at stirring rates of 100 to 150 rpm. ([10], chapter 16.3.4). Recently, Scholz et al. studied the dissolution performance of micronized and coarse grade felodipine in a biorelevant medium using the USP paddle apparatus at various paddle speeds [86]. Ratios of percentage dissolved were calculated pairwise for slower as well as for faster stirring rates. These ratios were then compared to AUC ratios obtained in a corresponding pharmacokinetic study in labradors, in which the absorption of both the micronized and coarse grade felodipine had been compared under two GI hydrodynamic conditions [86]. The authors proposed to use a paddle speed combination of 75 and 125 rpm to represent the motility patterns in response to administration of normal saline and 5 % glucose, respectively. *In vitro* AUC ratios of this particular experimental setup showed best agreement with the pharmacokinetic data [30]. It seems that the compendial paddle apparatus can be used both to simulate intestinal hydrodynamics as well as to reflect *variations* in hydrodynamic conditions in the upper GI tract.

9 Recommendations on the choice of an appropriate dissolution test apparatus

The following considerations may support the choice of an appropriate dissolution test apparatus based on different hydrodynamic scenarios *in vivo*. Constant flow rates, such as those that may occur in MMC phase I-II, in the regular fed state or at distal segments of the small intestine, are best simulated by the paddle method (Ph. Eur. 2002, 2.9.3.-1, USP apparatus 2). Dissolution is mainly driven by convection and the hydrodynamics of the paddle are easy to select and standardize. Thus, provided an appropriate composition, volume and particle size range are chosen for the dissolution test, the paddle apparatus can be used to reflect hydrodynamic conditions in the upper GI tract under certain dosing conditions [86]. However, if the flow rates to be reflected *in vitro* are varying with time (e.g. pulsatile flow rates of the MMC-phase III or transpyloric flow) the flow-through tester may be the more suitable apparatus since the flow rates *in vitro* can be varied with time using appropriate pumps and control software. At an early developmental stage it might sometimes be desirable to produce mechanical stress acting on the drug formulation *in vitro*. This could be required to simulate effects of the „antral mill“ (on the formulation) or of grinding by the intestinal wall (on particle agglomerates). In this case the drug release and the particle dissolution are furthered by erosion and thus increased by abrasive processes ([87] [10], with additional references). The best choice for this kind of application might be the „Biodis™“ apparatus. Alternatively, the paddle method could be appropriate, provided the vessels are filled with glass beads [88]. However, mechanical forces are only relevant for the dissolution of particle agglomerates and the drug release from formulations that are *susceptible* to mechanical stress, like HPMC matrix tablets. In contrast, erosion and abrasion play a minor role for smaller units like single drug particles or microparticles that are primarily subject to convective diffusion hydrodynamics.

Conclusion

Hydrodynamics in the upper GI tract contribute to *in vivo* dissolution. Our ability to forecast dissolution of poorly soluble drugs *in vitro* depends on our knowledge of and ability to control hydrodynamics as well as other factors influencing dissolution. Provided suitable conditions (apparatus, hydrodynamics, media) are chosen for the dissolution test, it seems possible to predict dissolution limitations to the oral absorption of drugs and to reflect variations in hydrodynamic conditions in the upper GI tract. The fluid volume available for

dissolution in the gut lumen, the contact time of the dissolved compound with the absorptive sites and the particle size have been identified as the main “hydrodynamic” determinants for the absorption of poorly soluble drugs *in vivo*. The influence of these factors is usually more pronounced than that of the motility pattern or the gastrointestinal flow rates *per se*.

References

1 Z. Ramtoola, O.I. Corrigan, Effect of agitation intensity on the Dissolution rate of indomethacin and indomethacin-citric acid compressed discs. Drug Dev. Ind. Pharm., 14 (15-17) (1988) 2241-2253.

2 M.A. Raines T.A. Dewers, Mixed transport / reaction control of gypsum dissolution kinetics in aqueous solutions and initiation of gypsum karst. Chemical Geology, 140 (1-2) (1997) 29-48.

3 Z. Liu, W. Dreybrodt, Dissolution kinetics of calcium carbonate minerals in H2O-CO2 solutions in turbulent flow - The role of the diffusion boundary layer and the slow reaction H2O+CO2<->H++HCO3--. Geochimica et Cosmochimica Acta, 61 (14) (1997) 2879-2889.

4 E. Brunner, Reaktionsgeschwindigkeit in heterogenen Systemen. Z. Physik. Chem., 47 (1904) 56-102.

5 W. Nernst, Theorie der Reaktionsgeschwindigkeit in heterogenen Systemen. Z. Physik. Chem., 47 (1904) 52-55.

6 A.A. Noyes W.R. Whitney, Ueber die Auflösungsgeschwindigkeit von festen Stoffen in ihren eigenen Lösungen. Z. Physik. Chem., 23 (1897) 689-692.

7 A. Schükarew, Reaktionsgeschwindigkeiten zwischen Metallen und Haloiden. Z. physik. Chem., 8 (76) (1891) 76-82.

8 D.M. Levins J.R. Glastonbury, Particle-liquid hydrodynamics and mass transfer in a stirred vessel. Trans. Instn. Chem. Engrs., 50 (1972) 132-146.

9 V.G. Levich. (1962) Physicochemical hydrodynamics, 2. ed., Prentice Hall, Englewood Cliffs, New Jersey.

10 S.M. Diebold. (2000 / 2022). Hydrodynamik und Lösungsgeschwindigkeit - Untersuchungen zum Einfluß der Hydrodynamik auf die Lösungsgeschwindigkeit schwer wasserlöslicher Arzneistoffe. (*Hydrodynamics and Dissolution - Influence of Hydrodynamics on Dissolution Rate of Poorly Soluble Drugs*). Revised and supplemented version, Aachen / Jungingen: doi.org/10.5281/zenodo.8340011 (or) doi.org/10.34657/11456.

11 T.K. Sherwood B.B. Woertz, The role of eddy diffusion in mass transfer between phases. Trans. Amer. Inst. Chem. Eng., 35 (1939) 517-540.

12 L.N. Plummer T.M.L. Wigley, The dissolution of calcite in CO2-saturated solutions at 25°C and 1 atmosphere total pressure. Geochim. Cosmochim. Acta, 40 (1976) 191-202.

13 D.J. Tritton. (1995) Physical Fluid Dynamics, 2. ed., Oxford University Press, Oxford.

14 H. Blasius, Grenzschichten in Flüssigkeiten mit kleiner Reibung. Z. Math. Phys., 56 (1908) 1-37.

15 V.G. Levich, Theory of concentration polarization. J. Phys. Chem., 18 (9) (1944) 335-355.

16 A.W. Larhed, P. Artursson, J. Grasjo E. Bjork, Diffusion of drugs in native and purified gastrointestinal mucus. J. Pharm. Sci., 86 (6) (1997) 660-665.

17 J.H. De Smidt, M. Grit D.J.A. Crommelin, Dissolution kinetics of griseofulvin in mixed micellar solutions. J. of Pharm. Sci., 83 (9) (1994) 1209-1212.

18 S.-H. Chang E.-L. Parrot, Hydrodynamics of dissolution in a newtonian and a non-newtonian solution. Drug Dev. Ind. Pharm., 17 (13) (1991) 1731-1751.

19 M.L. Dundon E. Mack, The solubility and surface free energy of calcium sulfate. J. Am. Chem. Soc., 45 (11) (1923) 2479-2485.

20 P.S. Roller, Chemical activity and particle size. II. The rate of solution at slow stirring of anhydrite and gypsum. J. Phys. Chem., 36 (1932) 1202-1231.

21 H. Grijseels C.J.d. Blaey, Dissolution at porous interfaces. Int. J. Pharm., 9 (1981) 337-347.

22 R.G. Compton, P.J. Daly W.A. House, The Dissolution of Iceland Spar Crystals; The Effect of Surface Morphology. Journal of Colloid (and) Interface Science, **113** (1986) 12-20.

23 W. Dreybrodt D. Buhmann, A mass transfer model for dissolution and precipitation of calcite from solutions in turbulent. Chemical Geology, (1991) 107-122.

24 H. Schlichting. (1951) Grenzschicht-Theorie, G. Braun Verlag, Karlsruhe.

25 V.G. Levich, The theory of concentration polarisation. Acta Physicochim. U.R.S.S, 17 (5-6) (1942) 257-307.

26 S.D. Mithani. (1998) Dissolution and Precipitation of Dipyridamole: Effect of pH and Bile Salt Concentration, Thesis, The University of Michigan, Michigan.

27 N. Kaneniwa N. Watari, Dissolution of slightly soluble drugs. I. Influence of particle size on dissolution behaviour. Chem. Pharm. Bull., 22 (8) (1974) 1699-1705.

28 R.M. Atkinson, C. Bedford, K.J. Child E.G. Tomich, Effect of particle size on blood griseofulvin levels in man. Nature, **193** (1962) 588-589.

29 M. Kraml, J. Dubuc R. Gaudry, Gastrointestinal Absorption of Griseofulvin: 2. Influence of Particle Size in Man. Antibiot. Chemother., 12 (1962) 239-242.

30 A. Scholz, B. Abrahamsson, S.M. Diebold, E. Kostewicz, B.I. Polentarutti, A.-L. Ungell J.B. Dressman, Influence of hydrodynamics and particle size on the absorption of felodipine in labradors. Pharm. Res., 19 (1) (2002) 42-46.

31 E.K. Anderberg, M. Bisrat, C. Nyström, Physicochemical aspects of drug release. VII. The effect of surfactant concentration and drug particle size on solubility and dissolution rate of felodipine, a sparingly soluble drug. Int. J. Pharm., 6 (1988) 67-77.

32 P. Harriott, Mass transfer to particles. I. Suspended in agitated tanks. AIChEJ, 8 (1) (1962) 93-101.

33 P.M. Armenante, D.J. Kirwan, Mass transfer to microparticles in agitated systems. Chem. Eng. Sci., 44 (12) (1989) 2781-2796.

34 G.K. Batchelor, Mass transfer from small particles suspended in turbulent fluid. J. Fluid Mech., 98 (3) (1980) 609-623.

35 S.M. Diebold, J.B. Dressman, Dissolution of microparticles - A hydrodynamically based contribution to an unresolved pharmaceutical issue. Pharm. Res., in prep. (2003).

36 M. Bisrat, C. Nyström, Physicochemical aspects of drug release. VIII. The relation between particle size and surface specific dissolution rate in agitated suspensions. Int. J. Pharm., 47 (1988) 223-231.

37 M. Bisrat, E.K. Anderberg, M.I. Barnett, C. Nyström, Physicochemical aspects of drug release: XV. Investigation of diffusional transport in dissolution of suspended, sparingly soluble drugs. Int. J. Pharm., 80 (1992) 191-201.

38 S.M. Diebold, J.B. Dressman, Hydrodynamik kompendialer Lösungsgeschwindigkeits-Testapparaturen: Paddle und Basket. Pharm. Ind., 63 (1) (2001) 94-104.

39 S. Cammarn, A. Sakr, Predicting dissolution via hydrodynamics: salicylic acid tablets in flow through cell dissolution. Int. J. Pharm., 201 (2000) 199-209.

40 C. Johnson, S.K. Sarna, R. Baytiyeh, V. Cowles, Y.-R. Zhu, G.L. Telford, A.M. Roza, M.B. Adams, Postprandial motor activity and its relationship to transit in the canine ileum. Surgery, 121 (2) (1997) 182-189.

41 R. Oberle, T.-S. Chen, C. Lloyd, J.L. Barnett, C. Owyang, J. Meyer, G.L. Amidon, The Influence of the Interdigestive Migrating Myoelectric Complex on the Gastric Emptying of Liquids. Gastroenterology, 99 (1990) 1275-1282.

42 O. Keinke, M. Schemann, H.J. Ehrlein, Mechanical factors regulating gastric emptying of viscous nutrient meals in dogs. Quart. J. Exp. Physiol., 69 (1984) 781-795.

43 P.J. Sirois. (1989) Size and density discrimination of nondigestible solids during emptying from the canine stomach: A hydrodynamic correlation., Thesis, The University of Michigan, Ann Arbor.

44 W. Brener, T.R. Hendrix, P.R. McHugh, Regulation of the gastric emptying of glucose. Gastroenterology, 85 (1983) 76-82.

45 P.R. McHugh, T.H. Moran, Calories and gastric emptying: a regulatory capacity with implications for feeding. Am. J. Physiol., 236 (1979) R 254-260.

46 P.R. McHugh, T.H. Moran, J.B. Wirth, Postpyloric regulation of gastric emptying in rhesus monkeys. Am. J. Physiol., 243 (1982) R 408-415.

47 J. Schirra, M. Katschinski, C. Weidmann, T. Schafer, U. Wank, R. Arnold, B. Goke, Gastric emptying and release of incretin hormones after glucose ingestion in humans. J. Clin. Invest., 97 (1) (1996) 92-103.

48 J.N. Hunt, J.L. Smith, C.L. Jiang, Effect of meal volume and energy density on the gastric emptying of carbohydrates. Gastroenterology, 89 (1985) 1326-1339.

49 J.A.L. Calbet, D.A. MacLean, Role of caloric content on gastric emptying in humans. J. Physiol., 498 (2) (1997) 553-559.

50 G.E. Vist, R.J. Maughan, The effect of osmolality and carbohydrate content on the rate of gastric emptying of liquids in man. J. Physiol., 486 (2) (1995) 523-531.

51 J.C. Meeroff, V.L.W. Go, S.F. Phillips, Control of gastric emptying by osmolality of duodenal contents in man. Gastroenterology, 68 (1975) 1144-1151.

52 J.H. Meyer, J.B. Dressman, A. Fink, G. Amidon, Effect of size and density on canine gastric emptying of nondigestible solids. Gastroenterology, 89 (1985) 805-813.

53 R. Notivol, I. Carrio, L. Cano, M. Estorch, F. Vilardell, Gastric emptying of solid and liquid meals in healthy young subjects. Scand. J. Gastroenterol., 19 (1984) 1107-1113.

54 F. Carbonnel, J.C. Rambaud, O. Mundler, R. Jian, Effect of energy density of a solid-liquid meal on gastric emptying and satiety. Am. J. Clin. Nutr., 60 (1994) 307-311.

55 H.A. Ziessman, F.H. Fahey, M.J. Collen, Biphasic solid and liquid gastric emptying in normal controls and diabetics using continuous acquisition in LAO view. Dig. Dis. Sci., 37(5) (1992) 744-750.

56 N. Takamatsua, L.S. Welageb, Y. Hayashic, R. Yamamotod, J.L. Barnette, V.P. Shah, L.J. Leskof, C. Ramachandran, G.L. Amidon, Variability in cimetidine absorption and plasma double peaks following oral administration in the fasted state in humans: correlation with antral gastric motility. Eur. J. Pharm. Biopharm., 53 (2002) 37-47.

57 M.A. Barreiro, R.D. McKenna, I.T. Beck, Determination of transit time in the human jejunum by the single-injection indicator-dilution technique. Am. J. Dig. Dis., 13 (3) (1968) 222-233.

58 A. Wald, C. Back, T.M. Bayless, Effect of caffeine on the human small intestine. Gastroenterology, 71 (5) (1976) 738-742.

59 J.W. Matshese, J.R. Malagelada, S.F. Phillips, Intestinal fluid flow and pancreatic enzyme output after mixed solid-liquid meals of different composition. Gastroenterology, 74 (1978) 1135.

60 I. Cobden, M.C.J. Barker, A.T.R. Axon, Gastrointestinal transit of liquids. Ann. Clin. Res., 15 (1983) 119-122.

61 V.J. Caride, E.K. Prokop, F.J. Troncale, W. Buddoura, K. Winchenbach, R.W. McCallum, Scintigraphic determination of small intestinal transit time: Comparison with the hydrogen breath technique. Gastroenterology, 86 (1984) 714-720.

62 O. Wisen, P.M. Hellström, C. Johansson, Meal energy density as a determinant of postprandial gastrointestinal adaption in man. Scand. J. Gastroenterol., 28 (1993) 737-743.

63 L. Beaugerie, B. Flourie, P. Marteau, P. Pellier, C. Franchisseur, J.-C. Rambaud, Digestion and Absorption in the Human Intestine of Three Sugar Alcohols. Gastroenterology, 99 (1990) 717-723.

64 R.L. Dillard, H. Eastman, J.S. Fordtran, Volume-Flow Relationship During The Transport Of Fluid Through The Human Small Intestine. Gastroenterology, 49 (1) (1965) 58-66.

65 P. Kerlin, A. Zinsmeister, S. Phillips, Relationship of Motility to Flow of Contents in the Human Small Intestine. Gastroenterology, 82 (1982) 701-706.

66 A.M. Stephen, A.C. Haddad, S.F. Phillips, Passage of Carbohydrate Into the Colon-Direct Measurements in Humans. Gastroenterology, 85 (1983) 589-95.

67 K.H. Soergel. (1971) in Gastrointestinal motility (Demling, L. and Ottenjann, R., eds.), pp. 81-92.

68 P. Trendelenburg, Physiologische und pharmakologische Versuche über die Dünndarmperistaltik. Archiv Exp. Pathol. Pharmakol., 81 (1917) 55-129.

69 A.M. Holgate, N.W. Read, Relationship between small bowel transit time and absorption of a solid meal. Dig. Dis. Sc., 28 (9) (1983) 812-819.

70 A. Miller, H.P. Parkman, J.C. Urbain, K.L. Brown, D.J. Donahue, L.C. Knight, A.H. Maurer, R.S. Fisher, Comparison of scintigraphy and lactulose breath hydrogen test for assessment of orocecal transit. Dig. Dis. Sci., 42 (1) (1997) 10-18.

71 J.H. Sellin, R. Hart, Glucose malabsorption associated with rapid intestinal transid. Am. J. Gastroenterol., 87 (5) (1992) 584-589.

72 M. Schemann, H.-J. Ehrlein, Postprandial Patterns of Canine Jejunal Motility and Transit of Luminal Content. Gastroenterology, 90 (1986) 991-1000.

73 M.G. Sarr, K.A. Kelly, Patterns of movement of liquids and solids through canine jejunum. Am. J. Physiol., 239 (1980) G 497-503.

74 N.J. Soper, K.L. Geisler, M.G. Sarr, K.A. Kelly, A.R. Zinsmeister, Regulation of canine jejunal transit. Am. J. Physiol., 259 (1990) G 928-933.

75 C. Johnson, S. Sarna, V. Cowles, R. Baytiyeh, Y.-R. Zhu, E. Buchmann, L. Bonham, A.M. Roza, M.B. Adams, Effects of transection and reanastomosis on postprandial jejunal transit and contractile activity. Surgery, 117 (1995) 531-537.

76 L. Bueno, J. Fioramonti, Y. Ruckebusch, Rate of flow of digesta and electrical activity of the small intestine in dogs and sheep. J. Physiol., 249 (1975) 69-85.

77 R.A. Hinder, K.A. Kelly, Canine gastric emptying of solids and liquids. Am. J. Physiol., 233 (1977) E 335-340.

78 C.H. Malbert, Y. Ruckebusch. (1990) in Gastro-pyloro-duodenal coordination (Nueten, J.M., Schuurkes, J.A.J. and Akkermans, L.M.A., eds.), 1. ed., Wrightson Biomedical Publishing, Petersfield.

79 R.C. Heading, P.M. King. (1990) in Gastro-pyloro-duodenal coordination (Nueten, J.M., Schuurkes, J.A.J. and Akkermans, L.M.A., eds.), 1. ed., Wrightson Biomedical Publishing, Petersfield.

80 P. Macheras, C. Reppas, J.B. Dressman. (1995) Biopharmaceutics of orally administered drugs, 1. ed., Ellis Horwood Ltd., Hemel Hempstead Hertfordshire, GB.

81 E.J. Beckers, N.J. Rehrer, W.H.M. Saris, F. Brouns, F.T. Hoor, A.D.M. Kester, Daily variation in gastric emptying when using the double sampling technique. Med. Sic. Exerc., 23(10) (1991) 1210-1212.

82 E.J. Beckers, J.B. Leiper, J. Davidson, Comparison of aspiration and scintigraphic techniques for the measurement of gastric emptying rates of liquids in humans. Gut, 33 (1992) 115-117.

83 M.G. Sarr, K.A. Kelly, S.F. Phillips, Canine jejunal absorption and transit during interdigestive and digestive motor states. Am. J. Physiol., 239 (1980) G 167-172.

84 N.S. Williams, J.H. Meyer, D. Jehn, J. Miller, A.S. Fink, Canine intestinal transit and digestion of radiolabeled liver particles. Gastroenterology, 86 (1984) 1451-1459.

85 B. Abrahamsson. (1997) Biopharmaceutical aspects of extended release tablets based on the hydrophilic matrix principle, Thesis, University of Uppsala, Uppsala (Sweden).

86 A. Scholz, E. Kostewicz, B. Abrahamsson, J. Dressman, Can the USP Paddle Method be Used to Represent In vivo Hydrodynamics? Pharm.Res, in press (2002) .

87 M. Kamba, Y. Seta, A. Kusai, K. Nishimura, Comparison of the mechanical destructive force in the small intestine of dog and human. Int. J. Pharm., 237 (2002) 139-149.

88 S. Aoki, H. Ando, K. Tatsuishi, K. Uesugi, H. Ozawa, Determination of the mechanical impact force in the in vitro dissolution test and evaluation of the correlation between in vivo and in vitro release. Int. J. Pharm., 95 (1993) 67-75.

89 V.D. Milton. (1982) An Album of Fluid Motion, (p 91), Parabolic, Stanford.

90 Institut für Plastination. (1997) Körperwelten, Einblicke in den menschlichen Körper (Ausstellungskatalog), Vol. 3., Institut für Technik und Arbeit, Heidelberg.

91 S.A. Riley, F. Sutcliffe, K. M., M. Kapas, M. Rowland, L.A. Turnberg, The influence of gastrointestinal transit on drug absorption in healthy volunteers. Br. J. Clin. Pharmac., 34 (1992) 32-39.

Tables

Tab 1. Mean flow rates (MFR) in various intestinal segments are related to the phase of the MMC in humans. Calculated according to Kerlin et al. (1982), Mean±SD, (From [10]).

MMC- Phase	MFR **Jejunum** (ml/min.)	**Ileum** (ml/min.)	**terminal. Ileum** (ml/min.)
I-II	0.58±0.12	0.17±0.03	0.33±0.01
III	1.28±0.18	0.50±0.13	0.65±0.01
Mean phase (I-III)	0.73±0.11	0.33±0.09	0.43±0.06
Fed state (400 ml)	3.00±0.67	2.35±0.28	2.09±0.16

Figures

Fig. 1: Laminar (A) and turbulent flow (B): t describes the time scale, U_A represents the velocity component acting in the direction of the flow. (From [10]).

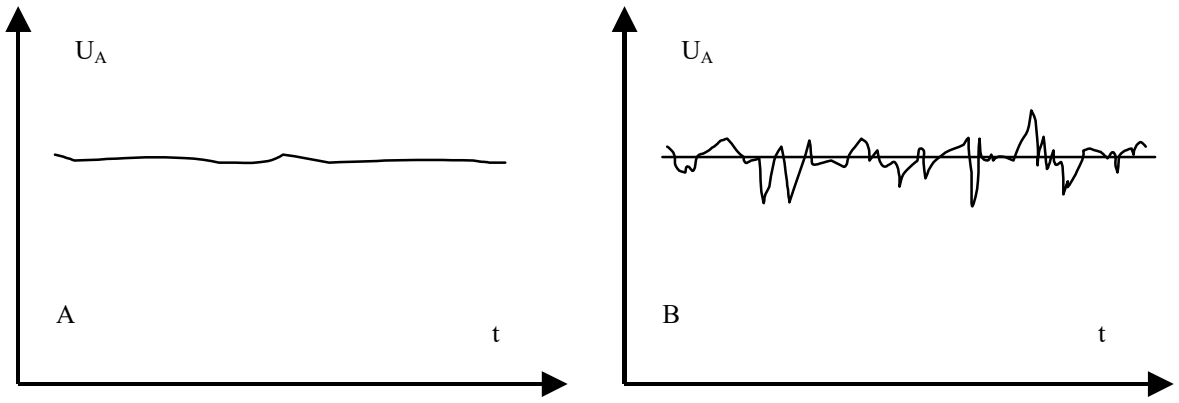

Fig. 2: „Eddies“ (large scale type) downstream of an object exposed to flow (Adapted from [13], § 21.4, original by Grant, H.L. (1958) J. Fluid. Mech. 4, 149)

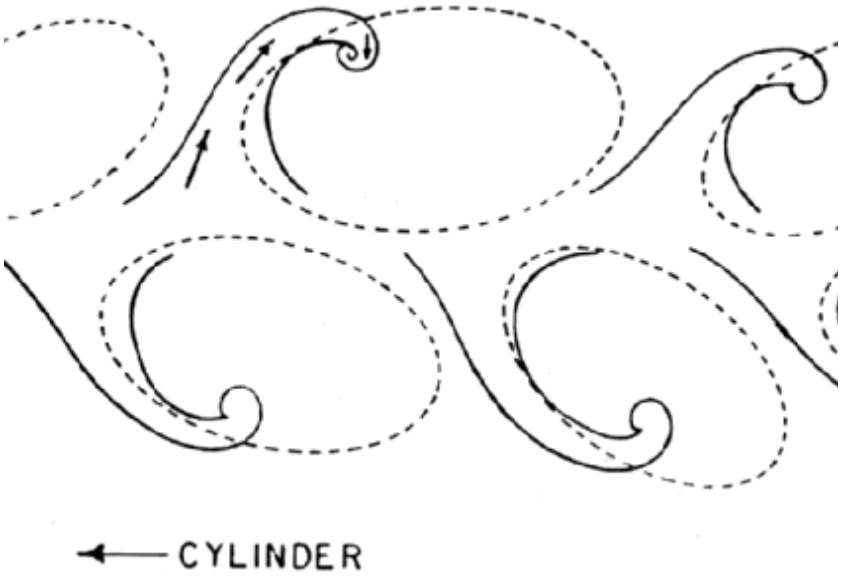

Fig. 3: Power input per unit mass of fluid: Paddle apparatus , 900 ml. Calculations shown for extremes of completely laminar and completely turbulent hydrodynamic conditions. The actual energy input lies in between the two curves, depending on the stirring rate. (From [10]).

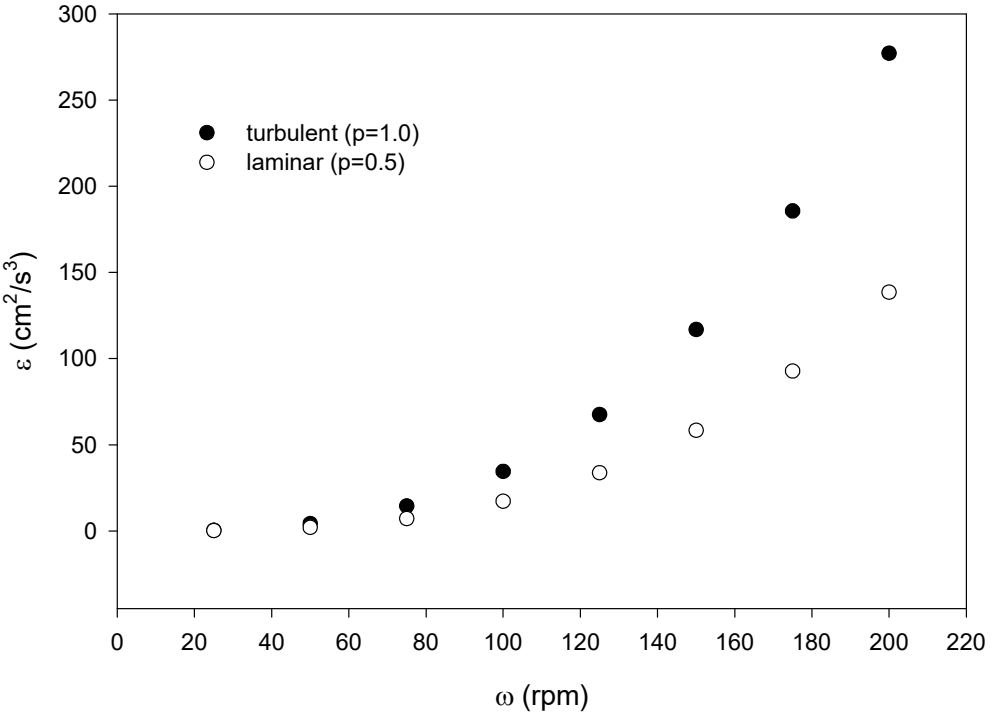

Fig. 4: Hydrodynamic boundary layer development on the semi-infinite plate of Prandtl (From [10]). δ_D = laminar boundary layer, δ_T = turbulent boundary layer, δ_{VS} = viscous turbulent sub-layer, δ_{DS} = diffusive sub-layer (no eddies are present, solute diffusion and mass transfer are controlled by molecular diffusion. The thickness is about 1/10 of δ_{VS}), B= point of laminar-turbulent transition.

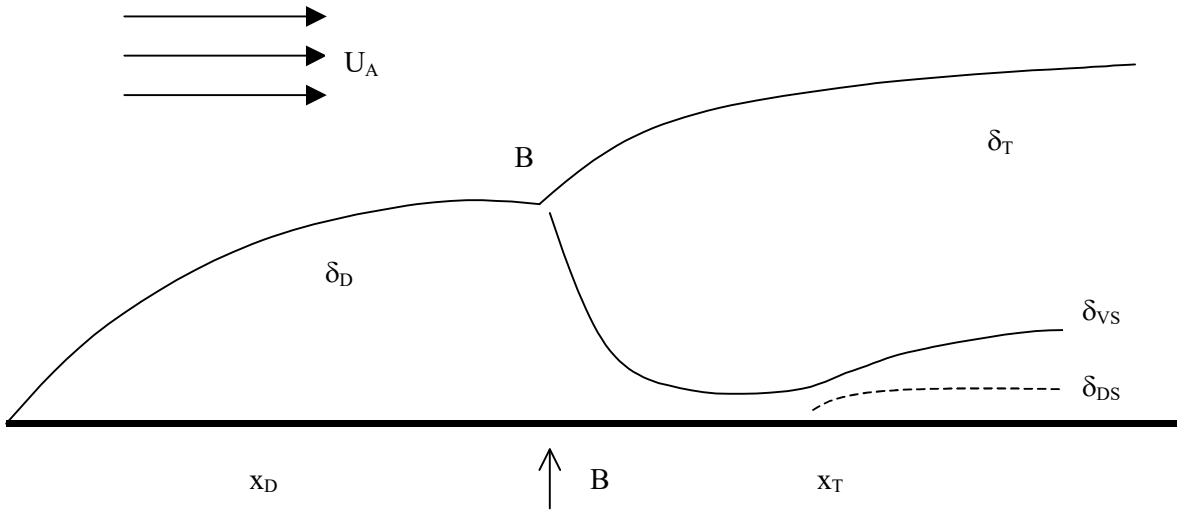

Fig. 5: Boundary layer separation: Turbulent versus laminar boundary flow close to an airfoil (From [89]).

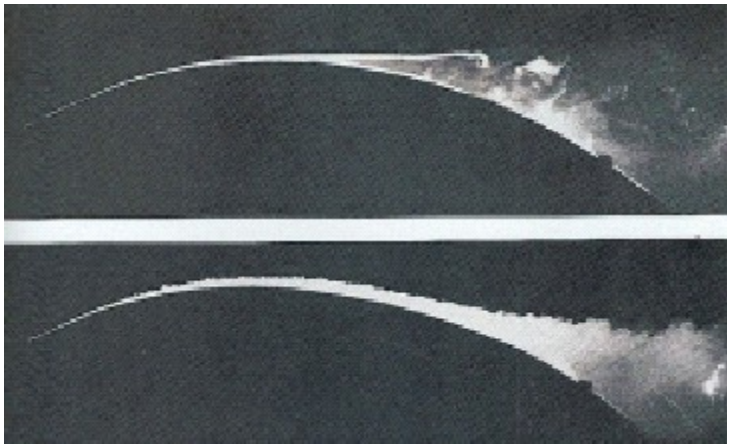

Fig: 6: Flow along a simulated surface roughness (protrusion type) at Re = 0.02, visualized using aluminium powder. Note the vortex generated at the downstream side of the cube. (Adapted from [13], § 12.1, original by Taneda, S. (1979), J. Phys. Soc. Japan, 46, 1935). Flow is from left to right as indicated by the arrow (added by the author).

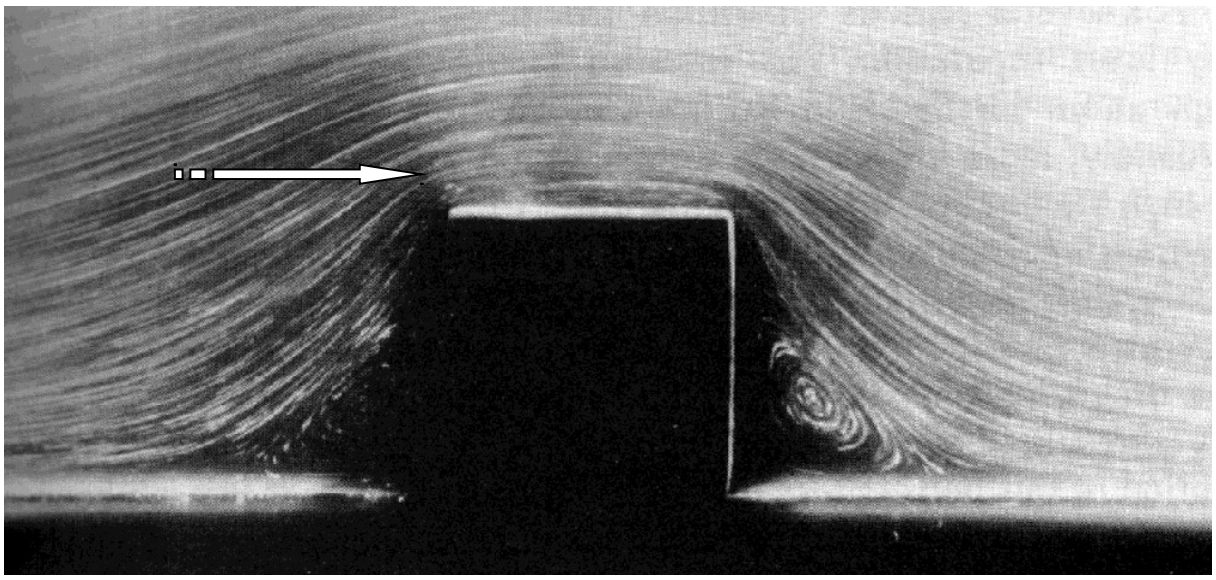

Fig. 7: Flow along an artificial cavitation at low Reynolds number (visualized using aluminium powder). Flow is from left to right. (Adapted from [13], § 12.4, original by Taneda, S. (1979), J. Phys. Soc. Japan, 46, 1935).

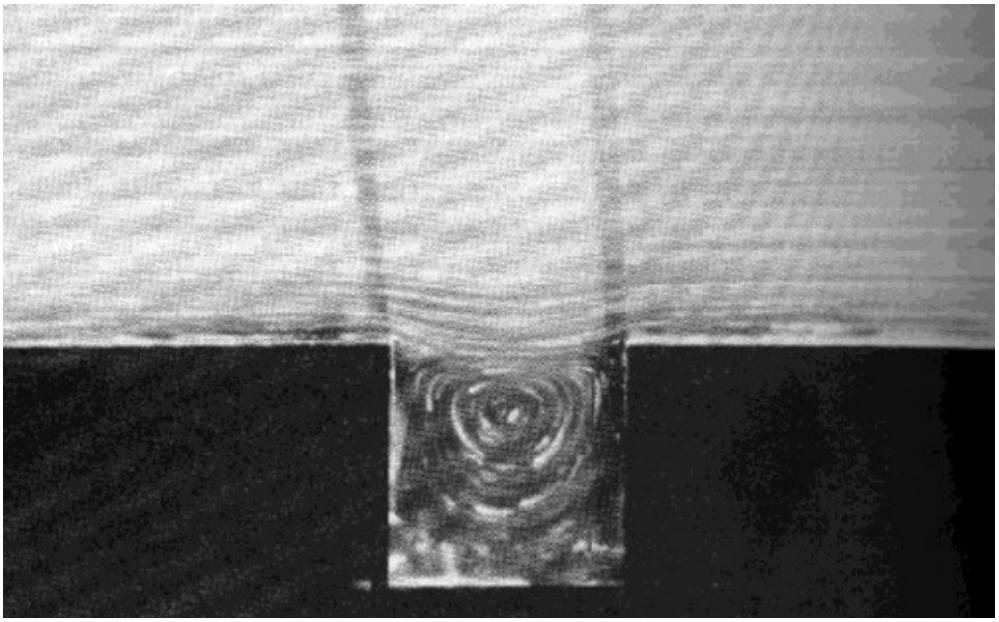

Fig 8: SEM-picture of a single felodipine crystal (coarse grade). The regular cube shows an apparently smooth surface. The arrow indicates the point at which the next picture (Fig. 9) was taken (From [10]).

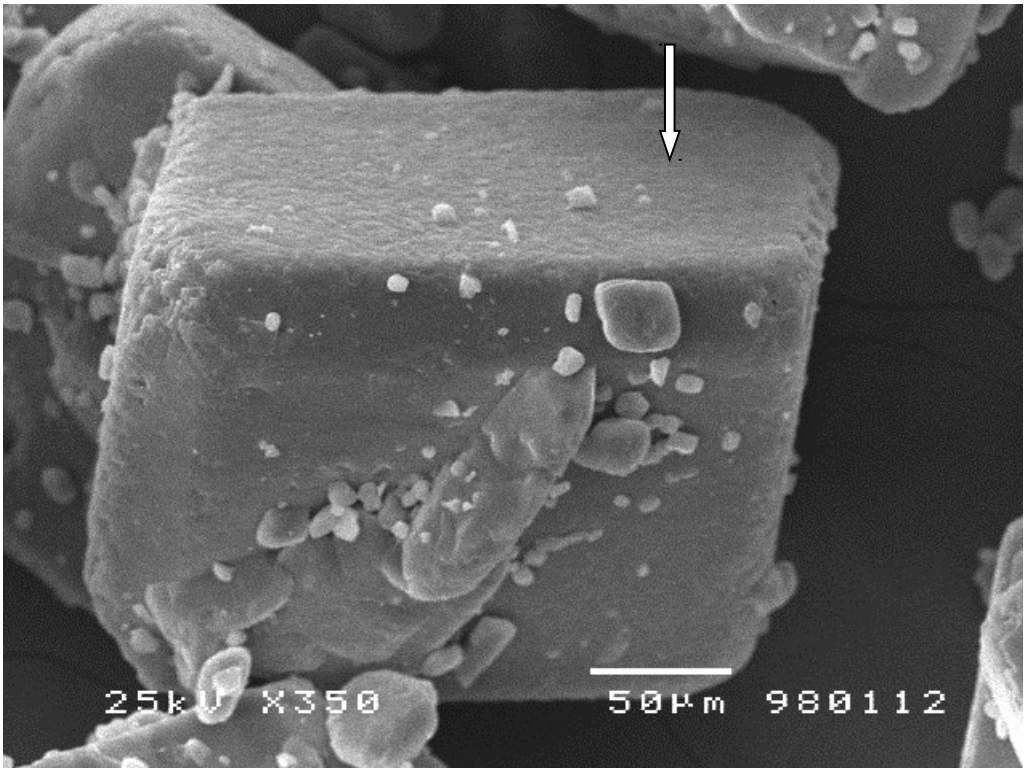

Fig. 9: SEM-picture of the surface of a smooth felodipine crystal apparently showing mounds, craters and hills (From [10]).

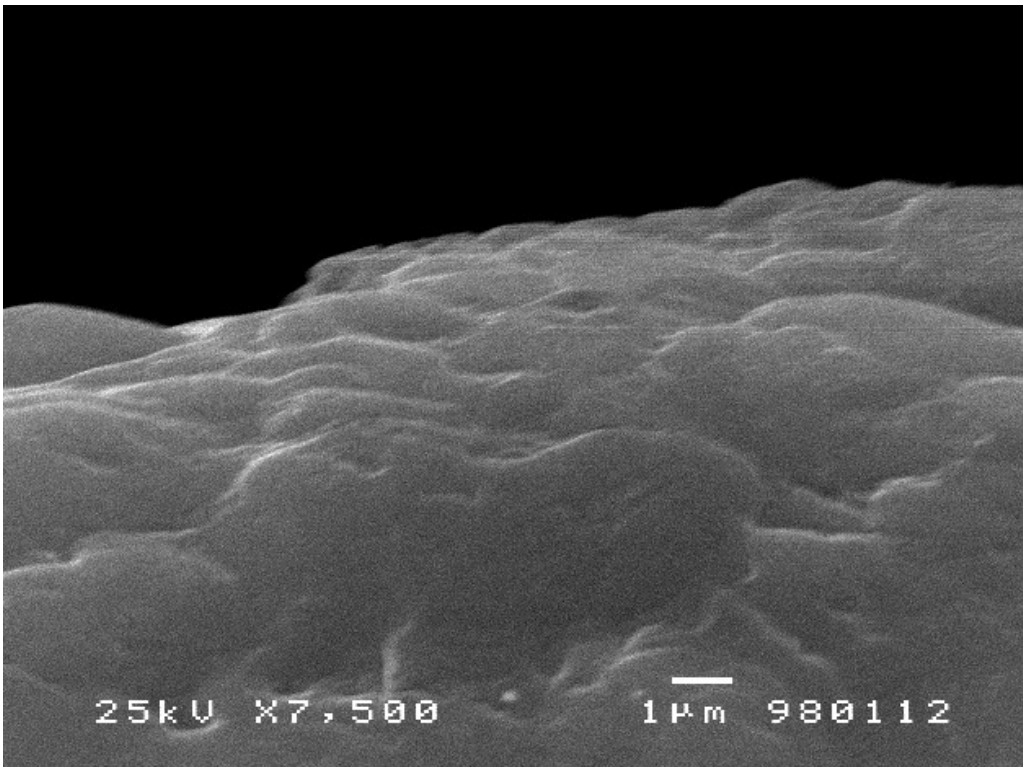

Fig. 10: Rotational (tangential) flow (U_A) as a function of stirring rate (ω) for paddle (filled circle) and basket (open circle): Mean±SD, position S2, approx. 1 cm above the paddle and midway between the paddle shaft and the wall of the dissolution vessel[4] (Data from [10], UPE-method).

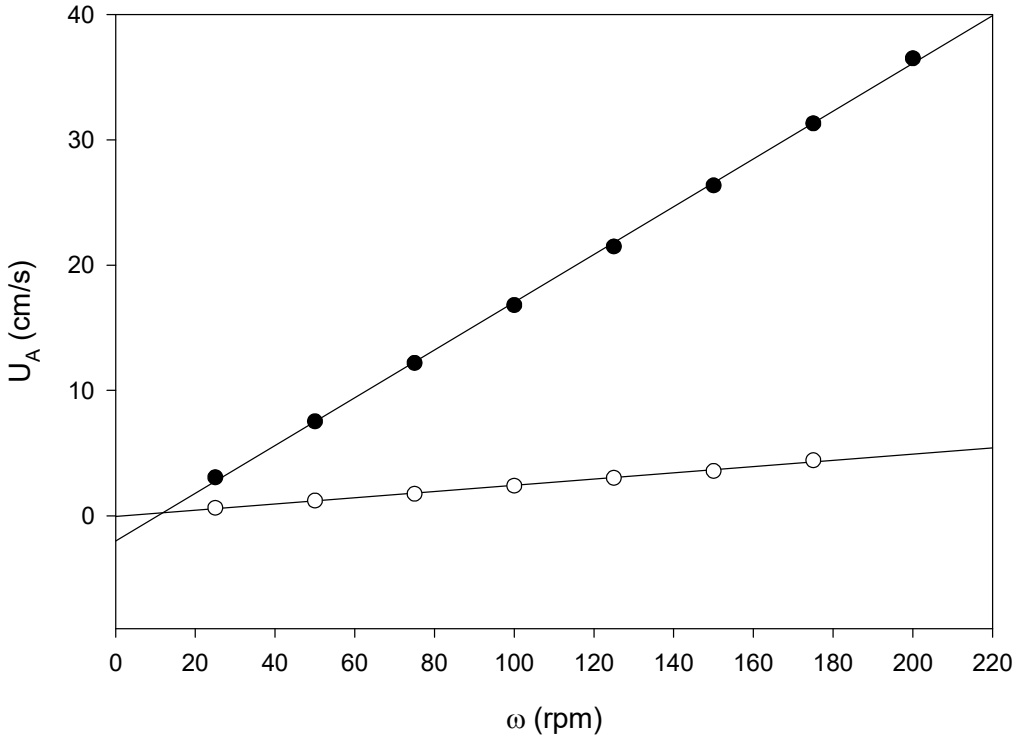

[4] Please note that, in contrast to simulation techniques like for instance "computational fluid dynamics", these data are based on dissolution experiments.

Fig. 11: Schematic flow pattern for the paddle apparatus (From [10])

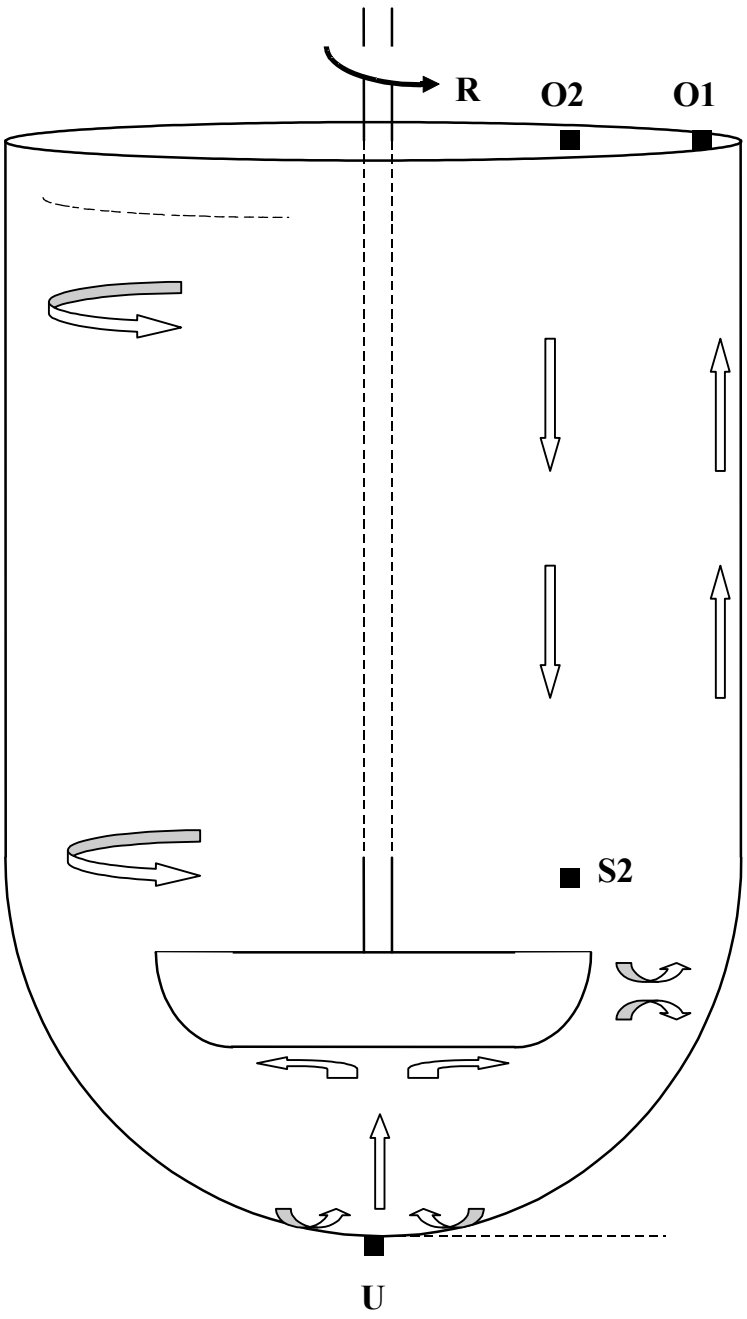

Fig. 12: Schematic flow pattern for the basket apparatus (From [10]). Because of the hemispheric designed symmetry of the dissolution vessel it is sufficient to draw the flow just for one half of the vessel. The arrows indicate flow direction. All designated flow patterns are based on *quantitative* experimental data.

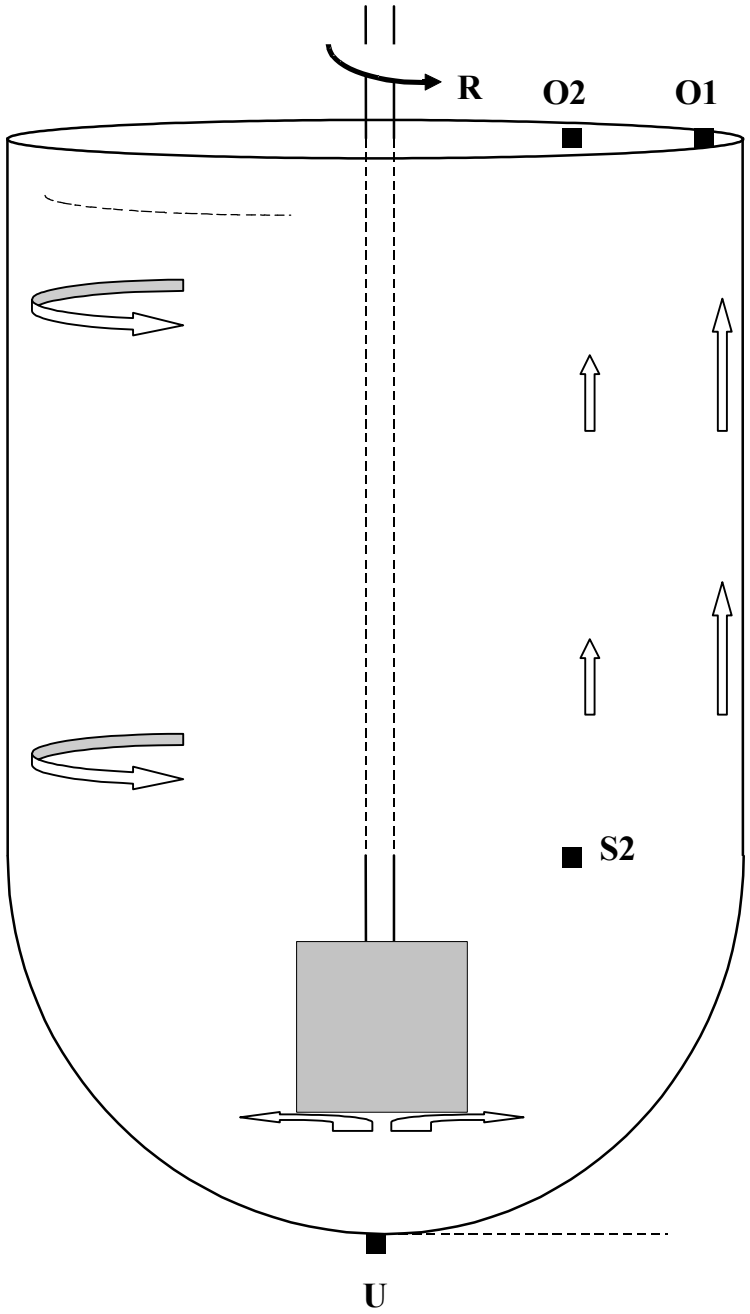

Fig. 13: Vertical (axial) flow (U_A) below the stirring device as a function of stirring rate (ω) for paddle (filled circle) and basket (open circle) at the bottom of the hemispheric dissolution vessel filled with 900 ml (From [10]).

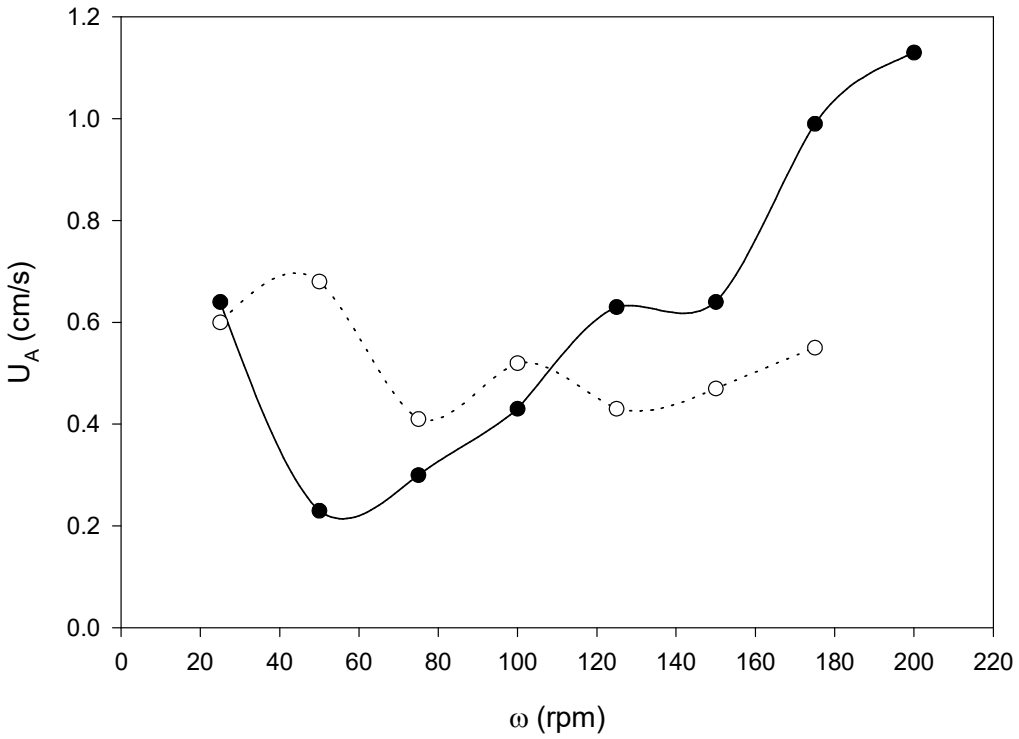

Fig 14. Vertical (axial) flow (U_A) above the stirring device as a function of stirring rate (ω) for paddle (filled circle) and basket (open circle): Mean±SD, vertical position O2 (From [10]).

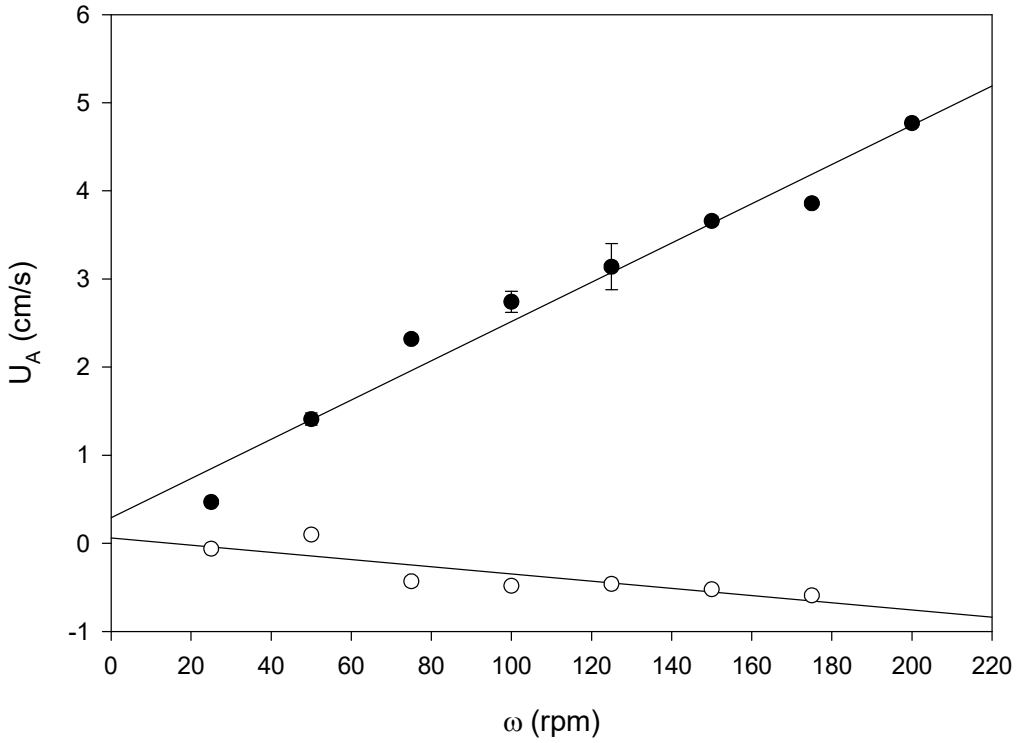

Fig. 15: Rotational (tangential) **flow (U_A) as a function of stirring rate (ω) for the basket using 900 ml (filled circle) and 500 ml (open circle): Mean±SD, n=6, P<0.001, paired t-test, lateral position S2 (From [10])**

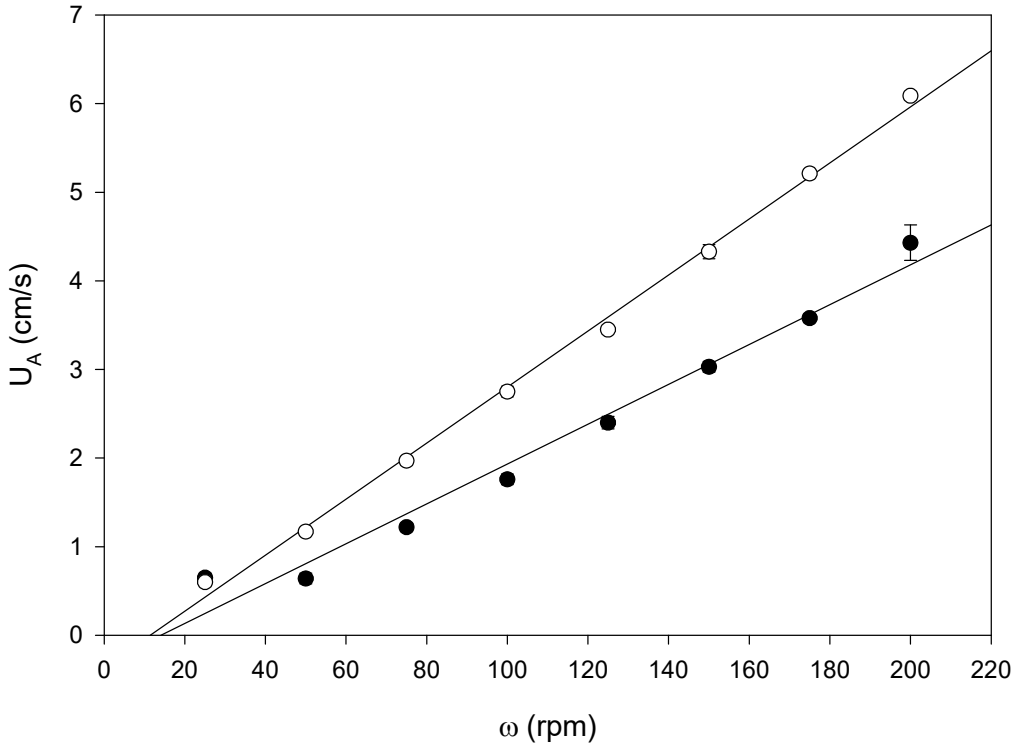

Fig. 16: Variability (time dependency) of differential gastrointestinal flow rates (DFR) in the small intestine of labradors. (V_R) represents the cumulative volume of chyme collected at midgut following oral administration of 200 ml glucose solution 20 % (I) and 200 ml NaCl 0.9 % (J), (From [10]).

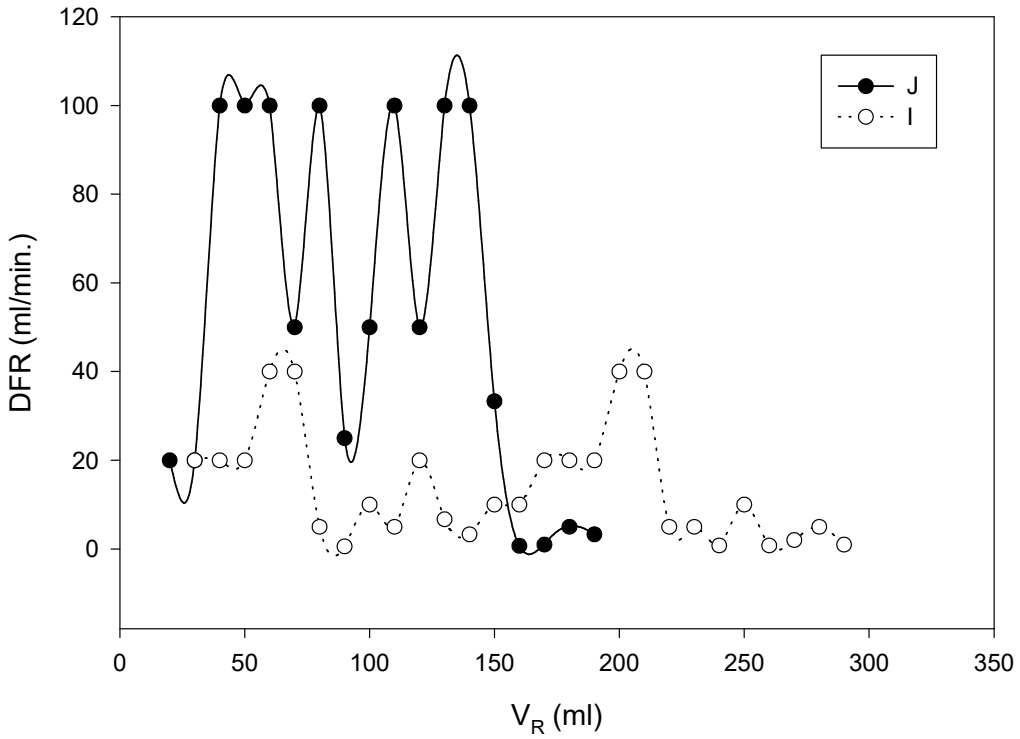

Fig. 17: Volume dependent *in vivo* dissolution of micronized felodipine: F_{CDNA} indicates the dissolved fraction of felodipine aspirated at mid-jejunum of labradors. The orally administered dose of 10 mg was suspended each in 200 ml saline 0.9 % (Experiments #E and #F) or glucose 20 % (Experiments ##B, D and S), respectively: V_R represents the recovered fluid volume (From [10], Fig 16.12)

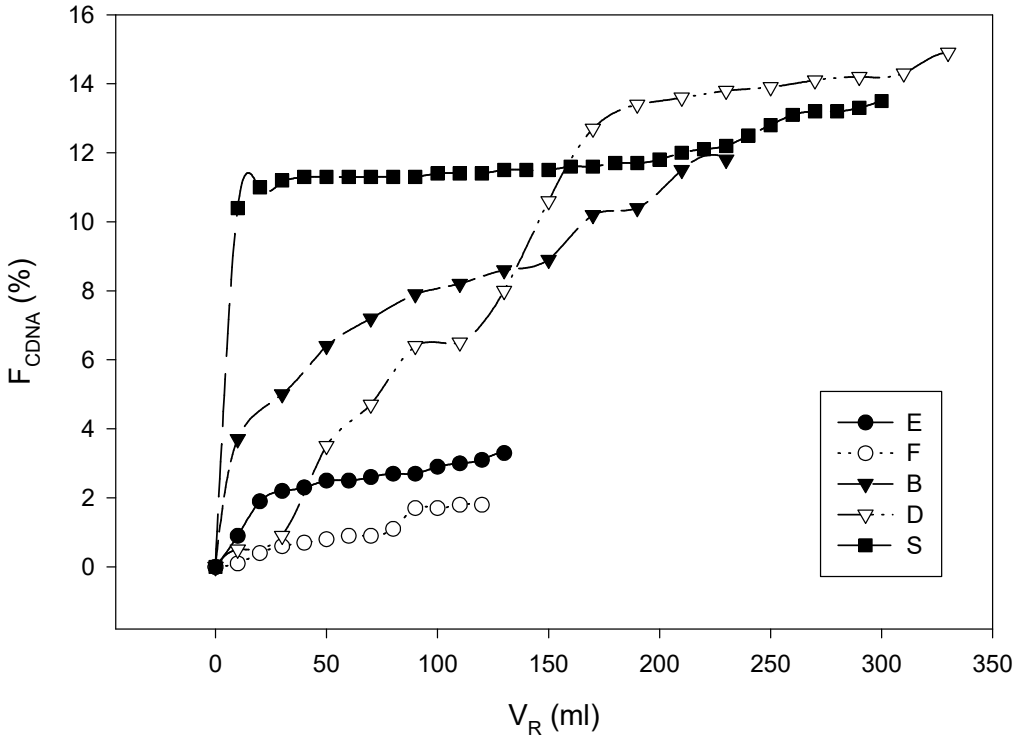

Fig. 18: Segment of the human small intestine with folds of mucous membrane (Prepared by plastination, from [90]). The total length of the human small intestine is estimated to be about 3.5 to 3.8 m.

Fig. 19: Mean plasma concentrations following the administration of felodipine suspension to Labradors: median particle size: 125 µm (n=6), dose: 10 mg, in either 0.9 % saline (NS) or 5 % glucose (Glc.) solution (From [30]).